Non-Covalent Interactions in N-Bromosuccinimide (NBS) & N-Iodosuccinimide (NIS) and their Role in Chemical Reactivity: A Matrix Isolation and *Ab Initio* Study

Jai Khatri

MS14004

A dissertation submitted for the partial fulfilment of

BS-MS dual degree in science

Indian Institute of Science Education and Research Mohali

May 2019

Certificate of Examination

This is to certify that the dissertation titled "Non Covalent Interaction Involving NBS & NIS and Their Role in Reaction Mechanism: A Matrix Isolation and *Ab Initio* Study" submitted by Mr. Jai Khatri (Reg.No.MS14004) for the partial fulfillment of BS-MS dual degree programme of the institute, has been examined by the thesis committee duly appointed by the institute. The committee finds the work done by the candidate satisfactory and recommends that the report be accepted.

Prof. K.S. Viswanathan	Dr. P. Balanarayan	Dr.Sugumar Venkataramani
(Supervisor)		

Dated: May __, 2019

Declaration

The work presented in this dissertation has been carried out by me with Prof. K.S. Viswanathan at the Indian Institute of Science Education and Research Mohali.

This work has not been submitted in part or in full for a degree, a diploma, or a fellowship to any other university or institute. Whenever contributions of others are involved, every effort is made to indicate this clearly, with due acknowledgement of collaborative research and discussions. This thesis is a bonafide record of original work done by me and all sources listed within have been detailed in the bibliography.

Jai Khatri
(Candidate)

Dated: May __, 2019

In my capacity as the supervisor of the candidate's project work, I certify that the above statements by the candidate are true to the best of my knowledge.

Prof. K.S. Viswanathan
(Supervisor)

Acknowledgements

I want to express my special thanks to my supervisor Prof. K.S. Viswanathan. I thank him for his continues encouragement throughout the project which not only helped me to grow as a researcher but also as a very strong person. His advice on both career as well as on my life have been priceless. I am very thankful to Dr. P. Balanarayan(committee member) for their help and discussion sessions throughout the entire thesis. I am also grateful to my committee member Dr. Sugumar Venkataramani for their insightful comments and suggestions during my project work. I also like to thanks Dr. Arijit kumar De. I want to thank Prof. Arvind Director, Prof. D.P. Sarkar, former Director and Prof. N. Sathyamurthy, former Director, IISER Mohali, for supporting me with all the facilities. I gratefully acknowledge DST for awarding me the INSPIRE scholarship for pursuing my BS-MS degree.

I owe my special thanks to Dr. Pankaj Dubey for being an amazing mentor, a friend and a colleague. I am very thankful to him, for always being there whenever I had any questions whether it is related to my work or not, he always helped in all scenarios. Without his guidance and discussions, the thesis would not have come to successful completion.

I also like to thanks to my other fellow lab members Dr. Jyoti, Himanshi and Shivangi for being very helpful and for maintaining a friendly and learning environment in the lab. If sugumar sir's lab weren't nearby to our lab, my project wouldn't be completed. So I owe my special thanks to Amandeep(Paji) very good friend & first lab partner, Mayank, Chitrnajan, Anjali, Virendra and Divyanshu for their funny way of doing all things (study, eating and imitating others). I also like to thanks from Balanaryan sir's lab Mr. Nitin and Rishabh(Guptaji). I also like to thanks to Bansal for being such a good friend and especially for the forcefully tea invitations. I also like to thanks some of my friends Shyam(techmaster), Monika(problem), Poonam(monitor), and Gulvinder(talker) for their support wherever I live they can't leave me. They were always there for me.

Last but not least, I would like to thank my parents, Mr. Mohan Khatri and Mrs. Rupa Khatri for their endless support. I also thank my brother Pankaj who were always very supportive of the in my whole life. Without all of them, I most certainly would not be where I am today.

Contents

3 Results and Discussion

List of Figures

List of Tables

List of Abbreviations

NBS	
NIS	N-Bromo Succinimide
	N-Iodo Succinimide
FTIR	Fourier Transform Infrared
Elec	Fourier Transform Infrared
ESP	Electrostatic
Dis	Electrostatic potential surface
Pol	Dispersive
Exch	Polarization
Rep	Exchange
UV	Repulsive
ESR	Ultra Violet
GM	Electron spin resonance
hυ	Gifford-McMahon
FCC	Sunlight
KBr	Face-centered cubic
NaCl	Potassium Bromide
CsI	Sodium Chloride
HF	Cesium Iodide
MP	Hartree-Fock
DFT	Møller–Plesset perturbation theory
SCF	Density Functional Theorem
M06-2X	Self- Consistent Field
FWHM	Minnesota functional
ZPE	Full width at half maximum
BSSE	Zero point energy
AIM	Basis Set Superposition Error
CP	Atoms-in-molecules
NBO	Critical point
EDA	Natural Bond Orbital
	Energy Decomposition Analysis

Abstract

The halogenation reactions have been extensively studied for many decades now. One of the oft used reagent for this reaction is N-Bromosuccinimide (NBS). For example, ethylene with NBS will yield a haloalkane. The mechanism of this was well known and is believed to proceed through the formation of a Bromonium ion as an intermediate. The question arises as to what is the driving force for the formation of the intermediate and in this thesis we explore the possibility of non-covalent interactions playing a role as a gateway for this intermediate.

We first studied the NBS-water interaction and followed it up with studies on the N-Iodosuccinimide (NIS)-water interaction. Our computations yielded five different complexes. While four of these were hydrogen bonded interactions, of these involved an oxygen-halogen interaction, which in the literature has been referred to as the halogen bond.

All *ab initio* computations were performed using M06-2X and MP2 methods with DGDZVP basis sets, using Gaussian-09 software. Interaction energies of the complexes were also computed using the same level of theory. Frequency calculations were performed to confirm if the structure corresponding to a stationary point is a minimum and to assign our experimental features. AIM and NBO calculations were done to understand the nature of the interactions in the complexes.

At the MP2/DGDZVP level, BSSE corrected interaction energies shows that the halogen bonded complex was the most strongly bound complex among all the minima in the NIS-water system. In the NBS-water system, the halogen bonded complex was only marginally less bound than the hydrogen bonded complex, indicating that this interaction could well play a role in the reaction mechanism. This work has therefore highlighted the important role of the halogen bonding complexes and its role in the halogenation reaction mechanism.

Chapter 1

Introduction

Intermolecular interactions:

Intermolecular interactions are important in that they often determine the chemical reactivity and physical properties of molecular systems[1]. There are several types of intermolecular interactions that are present between molecules. The four main intermolecular interactions which are likely to span most of the molecules are dipole-dipole interaction, London-dispersion interaction, hydrogen and halogen bonding interactions.

Dipole-Dipole interactions: These intermolecular interactions are those in which bonded atoms have a significant difference in their electronegativity; thus resulting in permanent dipole moments in molecules.

London- Dispersion Force: They is generated due to instantaneous dipoles in neighboring atoms formed by charge imbalance. This transient charge imbalance induces a dipole in the nearby molecules; causing an attraction between the instantaneous dipole and the induced dipole.

Hydrogen Bond: It is an attractive interaction between a hydrogen atom from a molecule or a molecular fragment X-H in which X is more electronegative than H, and an atom or a group of atoms in the same or different molecule, in which there is evidence of bond formation[2].

Halogen bond: It is a type of noncovalent interaction featuring the halogen atom as electron acceptor despite its higher electronegativity[3]. In this bond, the halogen atom becomes the sandwich between the two atoms just like the hydrogen bond like one atom behave as a donor and other as acceptor.

1.1 Halogen Bonding:

The Halogen bond is a unique type of non-covalent interaction in which halogen atom is attached to electron withdrawing atom A and accepts electron density from another atom D, groups or molecules. In some ways, it is analogs to hydrogen bond. This type of interaction can be represented by:

XB: A–X - - - -D

Here X is any halogen except fluorine[4]. It is directional and usually manifests a A-X-D bond angle of ~180°.

1.1.1 History

Robert Mulliken developed a theory on donor-acceptor complex, in 1950[5], which described the mechanism by which halogen bond formation occurs. The first experiment investigation for halogen bonding was reported by Hassel's group in 1954, after confirming the interaction between oxygen and bromine atoms using X-ray diffraction technique[6]. The term halogen bond came to be known when Durham and coworkers investigated the complex of CCl_4, CBr_4, with pyridine and anisole in 1978[7]. Politzer and Murray explained the high directionality of halogen bond by studying the distribution of electron density around halogen atom computationally in 2007[8] and defined the concept of a "σ-hole"[9].

1.1.2 Sigma hole

The term sigma hole was first introduced by Clark[9] for defining the halogen bonding interactions. As previously explained, the halogen bonding is an electrostatic attraction between the positive potential of halogen and the negative site of another molecule. The concept of a region of positive potential near a halogen atom is counterintuitive. The central concept behind the positive potential is when a half-filled p orbitals on the halogen involves in forming a covalent bond, thus resulting in the electron deficiency on the outer region of that p orbital. This empty region of covalently bonded p orbital, which looks like a hole is called as σ-hole[9]. Such electron deficiency is sufficient for creating the possibility of electrostatic interaction with another molecule[10] carrying a negative site.

The definition of sigma hole also accounts for the directionality of halogen bonding and serves as the driving force in halogen bonding. The extent of halogen bonding also depends on the size of the sigma hole, which in turn depends on two factors. First, the electronegativity of the halogen atom[11], which is inversely related to the magnitude of sigma hole i.e. higher the electronegativity weaker the sigma hole. Second, the extent of sp hybridization of its unshared s valence electrons[11]. Therefore the strength of halogen bonding will increase as we go down in the halogen group of the periodic table[12]. Further σ hole is manifested on the halogen atom which is attached to strong electron withdrawing groups, such as CF_3, as in CF_3Cl and CF_3Br.

1.2 Halogenation reaction:

It is an addition reaction between unsaturated hydrocarbons and halogens. The classic and most common example of this is the reaction between an alkene and the dibromine in the presence of sunlight[13], as shown in Fig. 1.1

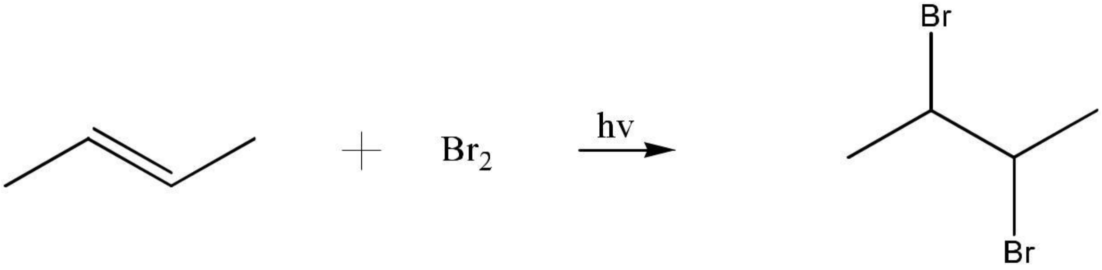

Fig1.1: Schematic representation of halogen addition reaction in the presence of sunlight using alkene as a precursor

The halogenation reaction is initiated with the formation of bromine radicals in the presence of sunlight. The bromine radicals formed then interact with unsaturated sites of alkene, through a free radical mechanism which generally involves the three-step initiation, propagation, and termination[14].

1.2.1 Reaction using NBS as a reagent

N-Bromosuccinimide (NBS) is white crystalline solid[15] and can act as halogenation reagent. The bromine attached to the electron withdrawing nitrogen of succinimide, results in bromine acquiring a partial positive charge, leading it to act as an electrophile. The reaction between an alkene and NBS forms a haloalkane, as shown in Fig 1.2 This is the classic example of electrophilic addition reaction in which NBS act as an electrophile and alkene as a nucleophile[16].

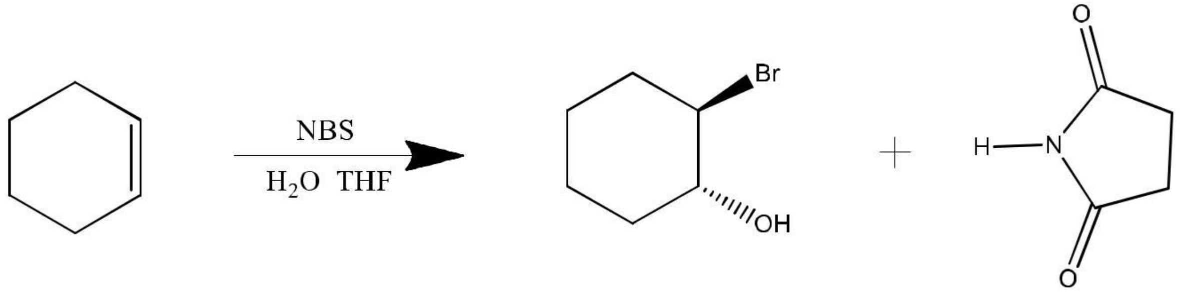

Mechanism:

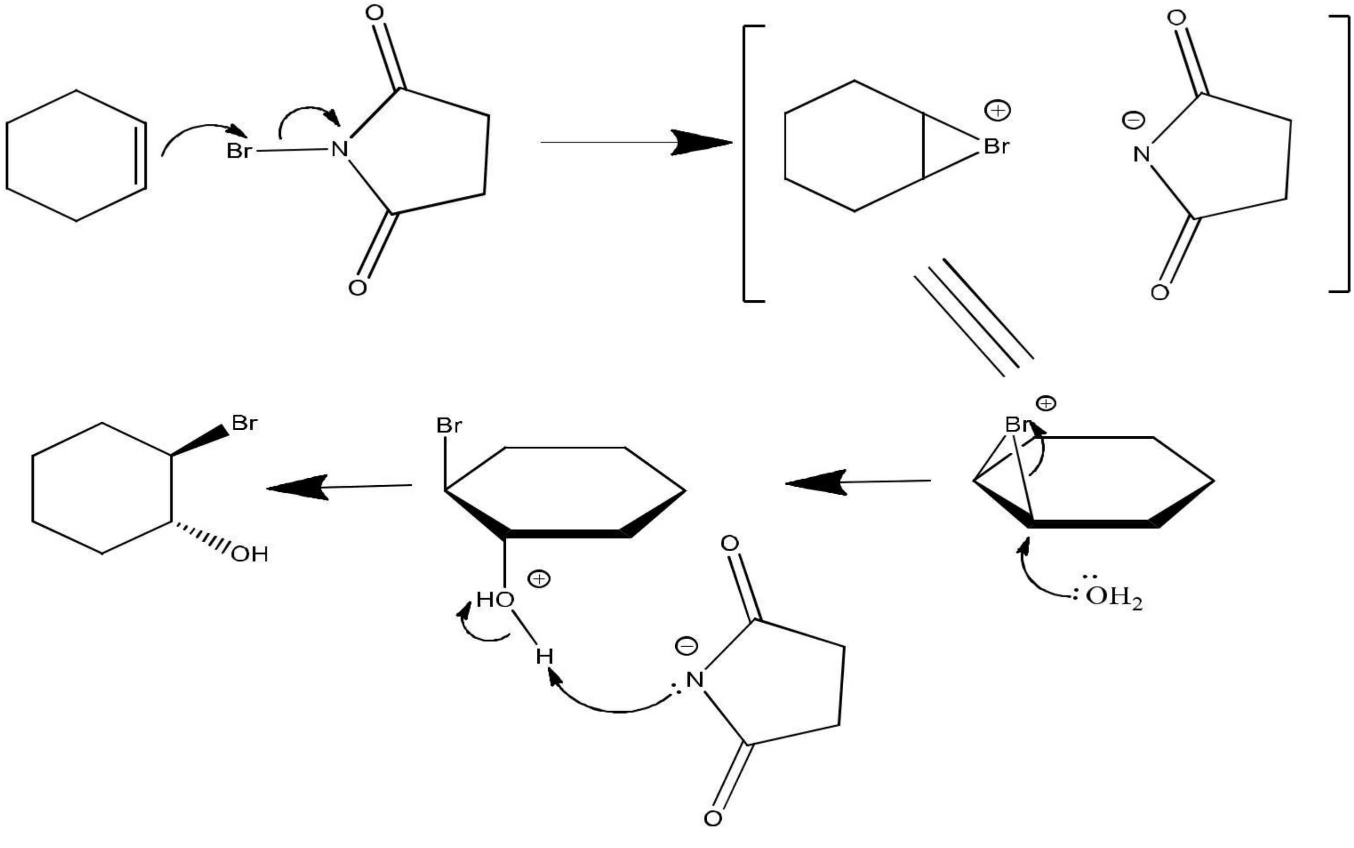

Fig. 1.2: Schematic representation of Halogenation reaction with the help of N-Bromo succinimide along with its mechanism.

The mechanism of halogenation reaction due to NBS is suggested to be driven by formation of bromonium ions. The nucleophilic alkene attack on bromine of NBS and forms a bromonium ion.

When water act as a solvent, it will attack the bromonium ion, resulting in the formation of halohydrin. In this reaction, the major product always is Trans, with respect to bromine and hydroxyl because of back side attack of water.

1.3 Motivation

Halogenation reaction is the one of the most important reaction in chemistry. At present the mechanism of halogenation reaction using NBS as a reagent is well defined. The intermediate of above reaction is bromonium ion was reported in literatures. While the formation of bromonium ion is still a debatable question. The alkene and bromine both are nucleophilic in nature, so who is attacking on who, in terms of chemistry, where is the electron going. Is it going from alkene to bromine or other way around? Who is behaving as electrophile and nucleophile?

All the questions arise led to one point what type of interactions present in between alkene and bromine, which type of complex that they are forming? Recently reported literatures shows that Bromine can act as electrophile due to presence of σ-hole. There is possibility that halogen bonding playing a role in the formation of bromonium ion. This thesis will address the question what is the force for the formation of bromonium ion.

In this thesis NBS-ethylene, NIS-ethylene and NBS –water were studied extensively to find the interaction between the NBS-ethylene using ab-initio calculations and matrix isolation infrared spectroscopy. Matrix isolation spectroscopy provides an excellent method to study the weak intermolecular interactions with multiple bonding sites, as is the technique is known to trap local minima, in addition to the global minimum.

Chapter 2

Experimental Setup and Computational Method

This chapter describes experimental aspects of matrix isolation infrared spectroscopy, and the computational methods employed to study the complexes of 1-Bromo-2,5-pyrrolidinedione (NBS) with water, ethylene and acetylene .

2.1 Matrix Isolation Technique

Matrix isolation spectroscopy is a technique where the sample molecules are trapped in a large excess of inert gas at very low temperatures. The typical inert gas to sample ratios are from 10^3:1 to 10^4:1 in order to achieve isolation of the molecule of interest in the inert matrix. The trapped species can be stable molecules or transient species, such as radicals, or ions.

This technique was first proposed and developed by George C. Pimentel[20] and G. Porter[21] in the 1950s, to study free radicals. Reactive species trapped in inert gas matrices have a long lifetime and hence can be easily studied by various spectroscopic techniques such as infrared, ESR[22] and UV-Visible[23] spectroscopy. The technique offers the advantages of small linewidths, which has made this technique a powerful and precise tool to study weakly bound complexes and conformations of molecules.

Inert gases such as neon, argon, and nitrogen are generally used in matrix isolation experiments. Furthermore, to be useful as a matrix material, there are various properties that material should satisfy. Some of the important properties are optical transparency in the region of interest, low volatility at the temperature of study of interest and acceptable thermal conductivity.

The matrix gas and the sample molecules are deposited on to a cold window, maintained at 10 K. The choice of the window depends on the spectral region used for the study. For mid-infrared region ranging from 4000-400 cm^{-1}, KBr or NaCl, whereas CsBr or CsI windows are used for the study in the far IR region, i.e., longer than 400 cm^{-1}. Quartz window are used for fluorescence and UV/visible spectroscopy. While this technique assumes that the molecules are trapped in an inert cage, in reality the matrix does interact weakly with the guest molecules. These very weak interactions between sample and inert matrix material were observed in the infrared spectra and manifest as matrix effects, which will be discussed in detail in a later section.

2.2 Advantages

In matrix isolation technique, the molecules are immobilized in the solid inert matrix; hence Doppler and collisions broadening are absent, and the linewidth becomes sharper. The sample to matrix ratios are also very high; hence the possibility of intermolecular interactions of the sample molecules are neglibible. Furthermore, the low temperature allows only the low rovibronic levels to be populated, which significantly reduces spectral congestion. For all the above reasons, the matrix isolated spectra are generally sharp, unlike the vapor phase and condensed phase spectra, which show very large linewidths and spectral congestion.

2.3 Matrix effects

Although the matrix is considered inert, in reality, matrix often perturbs the vibrational feature of trapped species, due to a variety of reasons. These matrix environmental effects are as follows:

2.3.1 Molecular Rotations

The molecules are tightly held and immobilized in the solid matrix with the low-temperature conditions inhibits the free rotations of sample molecules. However, for small molecules such as ammonia, water, and hydrogen halides, the rotations in inert matrices have been reported in the literature[24]. The rotational features of sample molecules can be identified by observing reversible intensity changes on temperature cycling.

2.3.2 Trapping Sites Effect

In general, when a molecule is trapped in a matrix, the geometrical structure of the site can perturb the spectrum feature. For the trapping site, we have to first discuss the crystal structure of the matrix itself. All the noble gases, except Helium, crystallize in face-centered cubic (FCC) lattices. In FCC crystal, each atom is surrounded by the 12 nearest equidistant neighbors.

The FCC crystal can have three possible guest sites; substitutional, in which accommodation of molecule can be done by removal of one, two or several matrix atoms depending on the guest size. The second is tetrahedral sites, for which the radius of the guest atom should be no larger than 0.225r (where r is the radius of matrix atom). The third is the octahedral site, where the radius of the guest atom should be no larger than 0.414r. Hence, most species will occupy a cage consisting of more than one substitutional site.

The weak intermolecular forces existing between the matrix and guest species will be different in different sites. Therefore, it is possible that different types of matrix cages and trapping sites may induce different vibrational frequencies, leading to the splitting of bands. The bands arising from the molecules trapped in stable sites can increase on annealing. Trapping the molecule in the different matrix also helps in the identification of bands due to multiple sites, since it is unlikely that two different matrices will give rise to similar trapping sites and wavenumbers.

2.3.3 Aggregation

Matrix isolation experiments are performed using the typical matrix to sample ratios of 1000:1 due to this molecular isolation is reasonably achieved. As the concentration of solute in matrix is increased, aggregates, such as dimers, trimers, and polymers may be formed and observed in addition to the monomers. The isolation depends on the size of the sample molecule because the probability of isolation is given by $P = (1 - r)^n$, where n is the number of matrix atoms surrounding the guest molecule.

2.3.4 Matrix shifts

The sample molecules trapped in the matrix under conditions of almost perfect isolation, do suffer from weak interactions with the matrix. These interactions can result either in a shift in the frequency or splitting of bands. The frequency shift ($\Delta\nu$) in a matrix with respect to the gas phase result from several types of interactions, such as electrostatic ($\Delta\nu_{elec}$), inductive ($\Delta\nu_{ind}$), dispersive ($\Delta\nu_{dis}$) and repulsive interactions ($\Delta\nu_{rep}$). The overall expression for frequency shift is given by the following expression,

$$\Delta\nu = (\nu_{matrix} - \nu_{gas}) = \Delta\nu_{elec} + \Delta\nu_{ind} + \Delta\nu_{dis} + \Delta\nu_{rep}$$

Where, ν_{matrix} and ν_{gas} are the frequencies of the vibrational mode of a molecule in the matrix and gas phase respectively[25].In inert gas matrices, the long-range London dispersion forces and the short-range repulsive forces are the two dominant interactions. The theoretical expression for frequency shift in solution with respect to gas arising from the perturbation due to solvent interactions is given by the Buckingham expression[26],

$$\Delta \nu = (\nu_{solvent} - \nu_{gas}) = [B_e/hc\omega_e]\ [U'' -$$

$3AU'/\omega_e$) Where, B_e is the rotational constant,

$c\omega_e$ = harmonic oscillator frequency for the normal

vibration, A = anharmonicity constant,

$U' = \delta U/\delta r_{bc}$ and $U'' = \delta^2 U/\delta r_{bc}^2$

U = energy due to solute and solvent interactions

2.4 Instrumentation Setup

The main components of matrix isolation setup involve low temperature cryostat, high vacuum system, and FTIR spectrometer, etc. The matrix isolation IR spectroscopy of our lab and its main components are shown in the following **Fig. 2.4**

2.4.1 Cryostat

The low temperature of 12 K required for matrix isolation studies is achieved using Sumitomo closed cycle helium compressor cooled cryostat (HC-4E1), which contains four main parts; a) Cold head b) Helium compressor c) Temperature control unit and d) Optical extension set.

2.4.1.1. Cold head and Helium compressor

The Main component of closed cycle cryostat is a cold head. It is connected to a compressor by two gas lines and electrical power cable. One of the gas lines supplies high-pressure helium gas to the cold head and other gas line returns the low-pressure helium gas from the cold head. The compressor provides the necessary helium gas pressure to achieve the low temperatures. The heat generated during the compression stageis dissipated by cold water provided by a chiller.

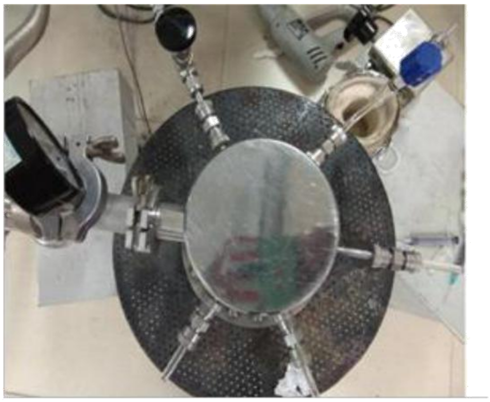

Fig. 2.2: Mixing chamber

Fig. 2.3: Temperature Controller

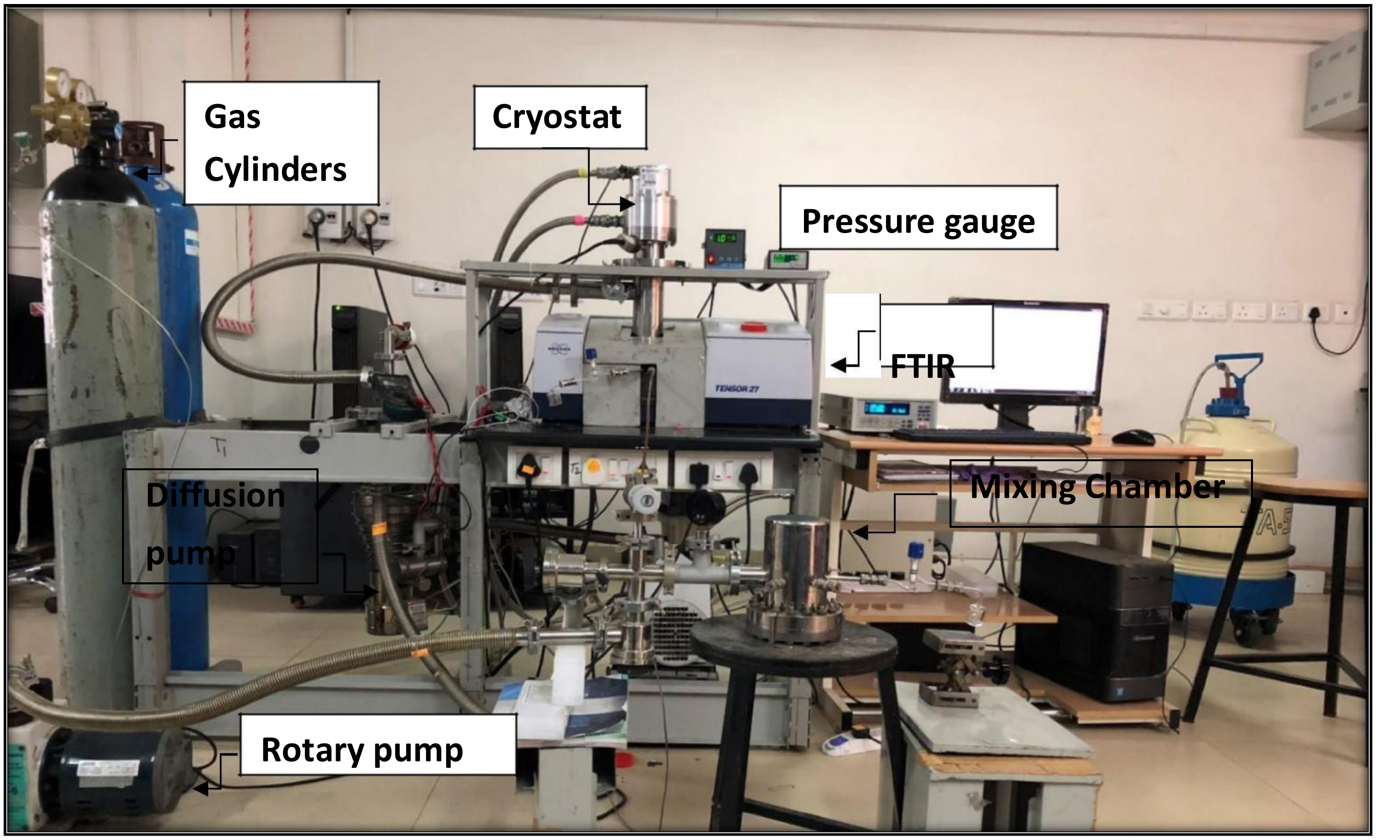

Fig. 2.4: Matrix Isolation Setup

Fig. 2.5: Helium Compressor

Fig. 2.6: Chiller

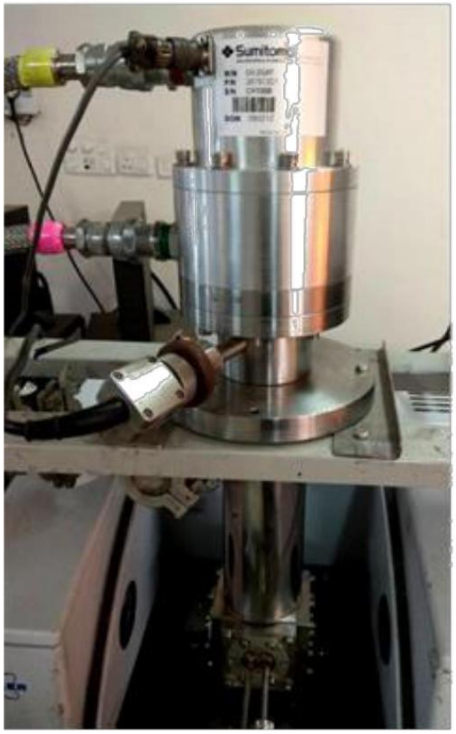

Fig. 2.7: Cryostat

Fig. 2.8: Diffusion Pump

The working principle of closed cycle cryostat based on the Gifford- Macmahon (GM) refrigeration cycle. The refrigeration cycle of the cryostat starts with the rotation of valve disk, which opens the path for high-pressure helium gas to pass through the regenerating material into the expansion space. Second, the pressure gradient drives the displacer allowing the gas at the bottom to expand and cool. Third, the rotation of the valve disk, which opens the path for low-pressure helium gas to flow through the regenerating material and removes heat from the system. The lowest temperature achieved by helium gas in GM cycle is around 10 K, and its schematic has been shown in Fig. 2.9:

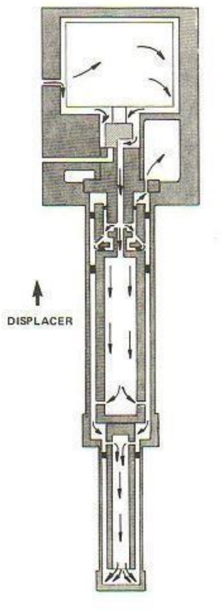

Fig2.9: The movement of High pressure He gas through the regenerating material

2.4.1.2 Temperature control unit

Temperature of the cryotip is measured using a silicon diode sensor. During annealing where temperatures above 12 K are required, a heater coil mounted on a cold tip is used. The current through the heater is regulated using a temperature control unit (Lakeshore 335 with PID controller). With this arrangement, the temperature can be varied from 12 K to 300 K.

2.4.1.3 Optical extension unit

The extension unit comprises into three part i.e. substrate holder, radiation shield and vacuum jacket. The substrate holder is attached to the cold head of cryostat, which attains a temperature of 12 K. A KBr substrate of 25 mm and 4 mm thickness is mounted on a cold substrate holder. Rotation shield made up of copper is fixed around the cryotip. The rotatable vacuum jacket has four ports, which is attached to another vacuum jacket through the O ring seal. KBr windows of 40mm diameter and 4 mm thickness were mounted on two of the opposite ports. Through these windows, the IR beam transmits to the inside KBr and then to the detector. The third port is fitted with a quartz window for viewing and to transmit UV-Visible light for photochemical studies when required. To the fourth port, an inlet system is connected through which the sample is deposited on the matrix.

2.4.2 Vacuum system

High vacuum (~ 10^{-6} mbar) is an important prerequisite both in terms of supporting the cryogenic setup to attain a low temperature and to ensure that species of interest are trapped without impurities. The cryostat is evacuated by an oil diffusion pump (Edwards, Diffstack MK2 series 100/300) with a pumping speed of 280 liters/sec, backed by a rotary pump. A second rotary pump (Hind Hivac) was used as a roughing pump for the vacuum system. Both rotary pumps have a pumping speed of 100 liters/min. The base vacuum in the system was 10^{-6} mbar, which is measured using a Penning gauge. Pressure in the region of 10^{-3} mbar or higher was measured using a Pirani gauge (Edwards APG 100 Active).

2.4.3 FTIR Spectrometer

The infrared spectrum of the matrix isolated species were recorded using a Bruker Tensor 27 FTIR spectrometer, operated at a resolution of 0.5 cm^{-1}. The number of scans recorded to observe spectral features with good signal to noise ratio ranged from 8 to 64.

2.4.4 Sample Introduction System

Matrix gas (Ar/N_2) was filled into a one-liter stainless steel mixing chamber, which was connected to the cryostat through a T-joint. While most experiments are usually performed using a nozzle maintained at room temperature, some of the experiments were performed using hot nozzle source (Fig 2.10), where the sample was heated to the desired temperature during deposition. This method had to be adopted where the sample has very low vapor pressure at room temperature, as in the case of NBS.

2.5 Experimental Procedure

The 1-Bromo-2,5-pyrrolidinedione (NBS) was taken into a hot nozzle shown in Fig. 2.10. The nozzle was heated by a constant DC power supply using Nichrome wires, placed around the sample holder. Water was loaded into glass blub, which was connected to the system high vacuum through a glass stopcocks. The water sample were thoroughly degassed before use, using several freeze-pump-thaw cycles. The cryostat was started and allowed to reach a temperature at 12K.

The temperature of the bath was maintained using a platinum resistance thermometer at an appropriate temperature to achieve the desired water:matrix ratio. The matrix and the samples are deposited onto the cold window and the flow rate of deposition was controlled using a needle valve. The flow rate of the matrix gas was usually maintained at ~3 mmol/hr.

After deposition the spectra were recorded at 12K. The matrix was then annealed, by raising the temperature of the matrix to ~32 K and maintaining at this temperature for about an hour. The matrix was then recooled to 12 K and a spectrum of the matrix thus annealed was recorded. The annealing temperatures employed was 32K in the case of Ar and 27K for N_2 matrix.

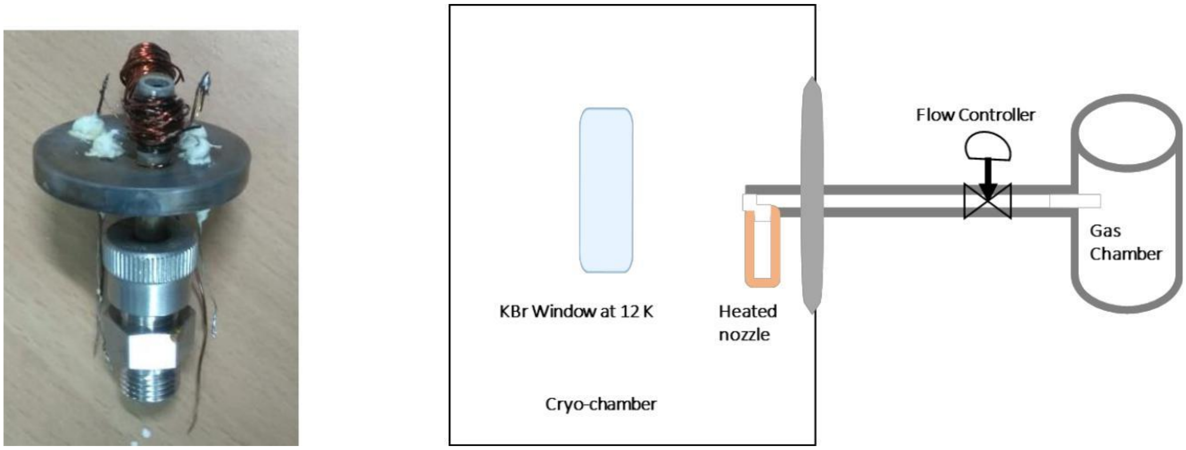

Fig. 2.10: Hot Nozzle with the sample holder and its working method in schematics

2.6 Computational Methods

Ab initio calculation has been carried out using the Gaussian 09 package for computational study. Molecular properties such as structures, energies, and frequencies were calculated to verify our experimental results. AIM (Atoms-In-Molecule) package was also used to examine the nature of the interactions between the monomers of complexes. Energy decomposition analysis calculation (EDA) has been carried out using GAMESS. A brief discussion regarding the computations is given below.

Some of the popular electron structure methods available for ab-initio calculations are Hartree-Fock methods (HF), Density Functional Theorem (DFT), Møller-Plesset perturbation theory (MP_n) (where n denotes the order of perturbation), Configuration interaction (CI), Coupled cluster (CC), Multi-configurational self-consistent field (MCSCF), etc.

DFT allows all electronic properties of the system to be determined from the electron density which is a function of three variables (x, y, z). One of such functional is BLYP (Becke-Lee-Yang-Parr) which includes some HF exchange. It involves both electron spin densities and their gradients. Hybrid functionals define the exchange functional as a linear combination of HF, local and gradient corrected exchange terms. The most used such functional is B3LYP. The B3LYP method uses the Becke-three parameter non-local exchange functionals with a non-local correlation of Lee. DFT includes electron correlation and hence more accurate than HF. Energy and orbital coefficients are solved by an iterative self-consistent field method. It is an appropriate method for systems having around 100 atoms. However, recently, advance modifications in DFT functionals have been introduced, such as Minnesota functional (M06). These are constraint satisfaction, modeling the exchange-correlation hole, empirical fits and mixing HF and approximate DFT exchanges. The M06-L, M06, M06-2X, and M06-HF are different type based on a different amount of HF exchange. There has another advancement in theory, Møller-Plesset perturbation theory (MP), which is a post HF ab-initio method. It improves on the HF method by adding electron correlation effects using Rayleigh-Schrodinger perturbation theory to second (MP2), third (MP3) and fourth order (MP4). This theory is more accurate with respect to experimental results but with a higher computational cost.

2.6.1 Geometry optimization and frequency Calculation

The stable structure of a molecule and complexes can be achieved by geometry optimization. Geometry optimization is an iterative self-consistent algorithm by which guess or initial geometry of molecules comes into an energetically stable configuration. A geometry optimization begins at the guess molecular structure specified as inputs, and the steps along the potential energy surface. The energy and gradient are first computed at the point on the potential surface corresponding to initial geometry. This information is used to determine how far and in which direction the next step is taken to improve the geometry. At the minimum or the stationary point, the forces will be zero. In case of Gaussian package, the optimization was achieved when the forces, the root mean square forces, the calculated displacement, and the root means square of the displacement for the subsequent step are below the preset threshold values, which depends on the level of theory and the restrictions.

The second derivative of the energy term at critical point determine the vibrational frequencies for the particular geometries. The vibrational frequencies calculation ensure that the computed structures did indeed correspond to minima on the potential surface. For a minimum, all frequency of vibration should be positive whereas, for saddle points, there can be imaginary frequencies for one or more modes of vibrations. Zero point vibrational energies (ZPE) were also obtained from frequency calculations which were used to calculate ZPE corrected energies.

2.6.2 Stabilization energy of complexes

The stabilization energy of the complex was computed using the method described below.

$$\Delta E = E_{AB} - (E_A + E_B)$$

Where, E_A, E_B, and E_{AB} represent the energies for monomers A, B, and the complex AB respectively. If the value of ΔE is negative, the complex is more stable relative to precursors. The stabilization energy of the complex with the zero points corrected energy (ZPE) was also calculated.

When the energy of complex (E_{AB}) is computed, the basis functions used are those of both the monomers subunits. Whereas, for computing the energy of individual monomers (E_A and E_B), the basis functions pertaining to only the corresponding monomers are used. As the number of basis function used is larger in the computation of complex, the energy obtained will be lower. Stabilization energies thus derived from the calculated energies E_A, E_B and E_{AB} will be overestimated, and the error is referred to as the basis set superposition error (BSSE). The best way to eliminate BSSE is to increase the basis set until the stabilization energy is stable to the desired accuracy. However, this procedure is seldom possible. The commonly used method to correct for BSSE is by counterpoise correction proposed by Boys and Bernadi. (Reference) In this scheme, the energies of both monomers and the complex are calculated using the same basis for the complex. Hozba and Halves have described the scheme of counterpoise corrected PES of H-bonded system[27]. The counterpoised BSSE correction can be expressed as follows

$$\Delta E = E_{complex}\text{ (complex basis)} - [E_A\text{ (complex basis)} + E_B\text{ (complex basis)}]$$

Stabilization energy is corrected individually for the ZPE and BSSE, as applying BSSE correction over the ZPE corrected energies estimated leads to an overestimation of interactions energies involved in the complex

2.6.3 Atoms-in-Molecule methodology

The atom in molecules theory is a method to observe the topology of electron density in space, locate bond paths and critical bond points for a system. This method was first proposed by Bader and his coworkers[18]. The wave function corresponding to the optimized geometry of a molecule or complex is generated using the Gaussian 09 package. From the electron density plots, one can obtain bond critical points, charge density $\rho(r)$, Laplacian of charge density$\nabla^2\rho(r_c)$, which is also the trace of Hessian of ρ. The charge density is a physical quantity which has a definite value at each point in space. It is a scalar field defined over three-dimensional space. Each topological feature of $\rho(r)$, where it is a maximum, a minimum, or a saddle point, has associated with it in a space called a critical point, where the first derivative of $\rho(r)$ vanishes. The topological properties of such a scalar field are conveniently summarized in terms of the number and nature of its critical points. The rank of the critical point, denoted as ω, is equal to several non-zero eigenvalues at the critical point. The signature (σ) is the algebraic sum of signs of eigenvalues.

The critical point is labeled by giving the values (ω, σ). For example, (3,-1) critical point means three non-zero curvatures and one positive and two negative eigenvalues. A (3, -1) critical point corresponds to a bond between two atoms, a (3, +1) critical point to a ring, a (3, +3) critical point to a cage and a (3, -3) critical point corresponds to a maximum.

The sum of three Hessians (λ_1, λ_2, λ_3) at a bond critical point is the Laplacian quantity. It is the characterization of the manner in which the electronic charge density is distributed in the internuclear region. If the value of charge density ρ ($<10^{-1}$ a.u.) and the curvature of charge density are large, Laplacian of charge density may be positive or negative usually in the same order of magnitude as $\rho(r_c)$ then the interaction is of shared type, typical of covalent interaction. For the closed shell interactions, such as hydrogen bond complexes, van der Waals complexes, and ionic systems, the charge density ρ ($\sim10^{-2}$ to 10^{-3} a.u.) at the bond critical point is quite small and the Laplacian of the charge density is positive.

2.6.4 Energy Decomposition Analysis

When a complex is formed between two monomers, it is essential to determine the different type of interactions involved in the complex. LMOEDA (write full name) divides the components of total interaction energy in terms of electrostatic energy, exchange value, repulsion energy, polarization energy and dispersion energy in a complex[28]. EDA helps us to understand the type of interactions which ultimately led to the formation of the complex; for example, hydrogen bonded interactions are primarily composed of electrostatic interactions. It was performed in GAMESS using the optimized geometries from Gaussian 09.

2.6.5 Natural Bond Orbital (NBO) Analysis

NBO determines the delocalization interactions involved in the stability of the complex. This can be calculated using the Gaussian 09 suite, which calculates the second order perturbation energies of the various donor-acceptor interactions involved in the complex. These orbital interactions are a function of energies difference between donor and acceptor, and the overlap is given by

$$E(2) = \Delta E_{ij} = \frac{q(i) . F(i,j)^2}{\varepsilon(j) - \varepsilon(i)}$$

Where q_i is the donor orbital occupancy, ε(j) and ε(i) is the diagonal elements, F(i,j) is the off-diagonal NBO Fock matrix elements, and E(2) is the second order perturbation energy.

Chapter 3

Results and Discussion

3.1 Computational Details

All the computational calculations (*ab initio)* were performed using MP2 and M06-2X methods and using DGDZVP[29] basis sets. N-Bromosuccinamide (NBS) and N-Iodosuccinamide (NIS) were optimized individually, and optimized geometries of these submolecules were then used for obtaining the optimized structure of the NBS-H_2O, NBS-acetylene, NBS-ethylene NIS-H_2O, NIS-acetylene and NIS-ethylene complexes. The electrostatic potential surface was calculated using optimized geometries of NBS and NIS and which are shown in Figure 3.1 The structure of the different complexes of NBS-H_2O, NIS-H_2O, NBS-acetylene and NBS-ethylene obtained at MP2/DGDZVP are shown respectively in Figure 3.3, 3.4, 3.5 and 3.6 along with the geometrical parameter listed in Table 3.1 and 3.2 respectively. To ensure all the complex are the minima, harmonic frequency calculation were done at the same level of theory. The frequency calculations were also useful for assigning the experimentally observed feature. The computed frequencies for all the complexes were positive, which confirmed that all the optimized structure were minima on the potential surface. The interaction energies were calculated using supermolecule[30] approach and were corrected using zero-point energy (ZPE) and basis set superposition error (BSSE) separately[31].

The computed frequency was scaled before assigning it to the experimentally observed features, in the following way. The strongest feature observed in the experiments was correlated with the strongest computed features for the monomers. The scaling factor was determined by taking the computed value of the submolecule and matched with its experimentally observed value; this scaling factor was then used to scale the computed frequencies of the complexes. In matrix isolation experiments, the matrix perturbs the different normal modes appearing in the different regions of the infrared region differently. Therefore, a mode by mode scaling was performed, where the above mentioned scaling procedure was followed to determine the scaling factor for the modes in the different spectral regions. The computed frequencies generated by using G09 software were plotted using graphical software, Gabedit[32]. The computed feature was plotted with Lorentzian lineshape and full width at half maximum (FWHM) of 2.0 cm^{-1}.

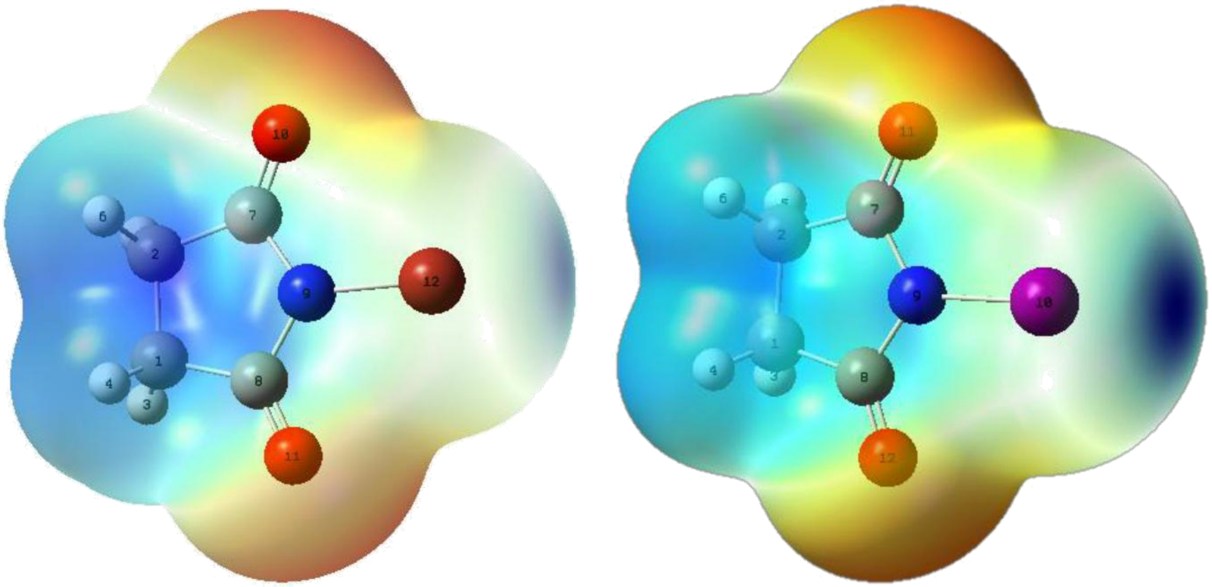

Figure 3.1: Electrostatic potential surface (ESP) of optimized geometries of NBS and NIS at MP2/DGDZVP.

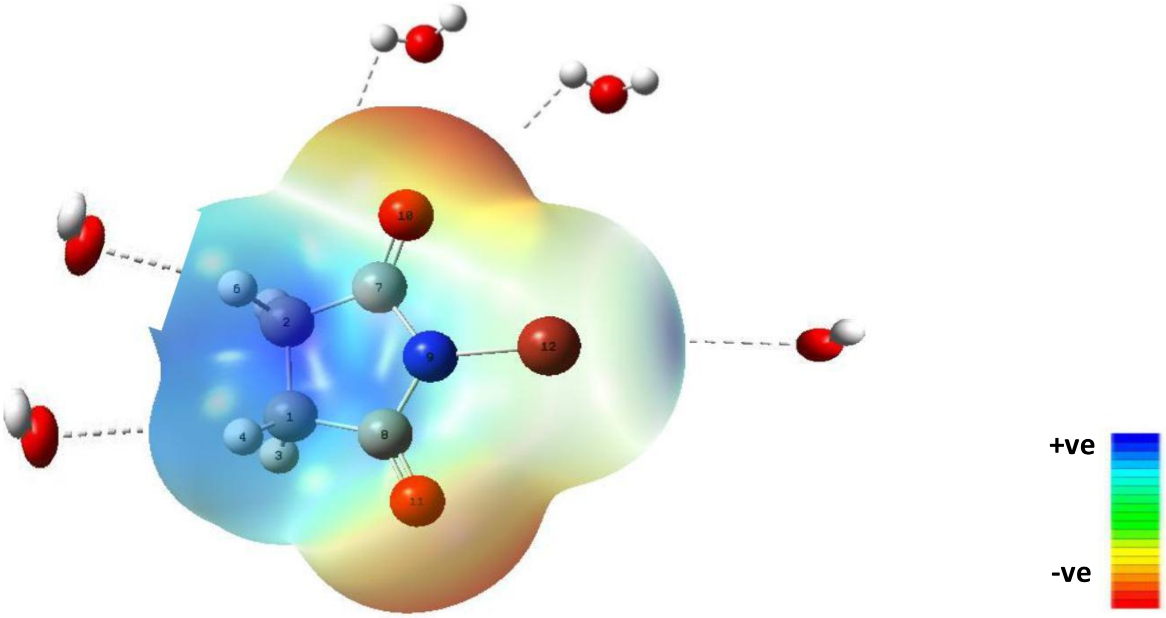

Figure 3.2: Electrostatic potential surface (ESP) of the optimized geometry of NBS with water for finding the different geometries. Along with the scale of ESP indicated in the right below a corner.

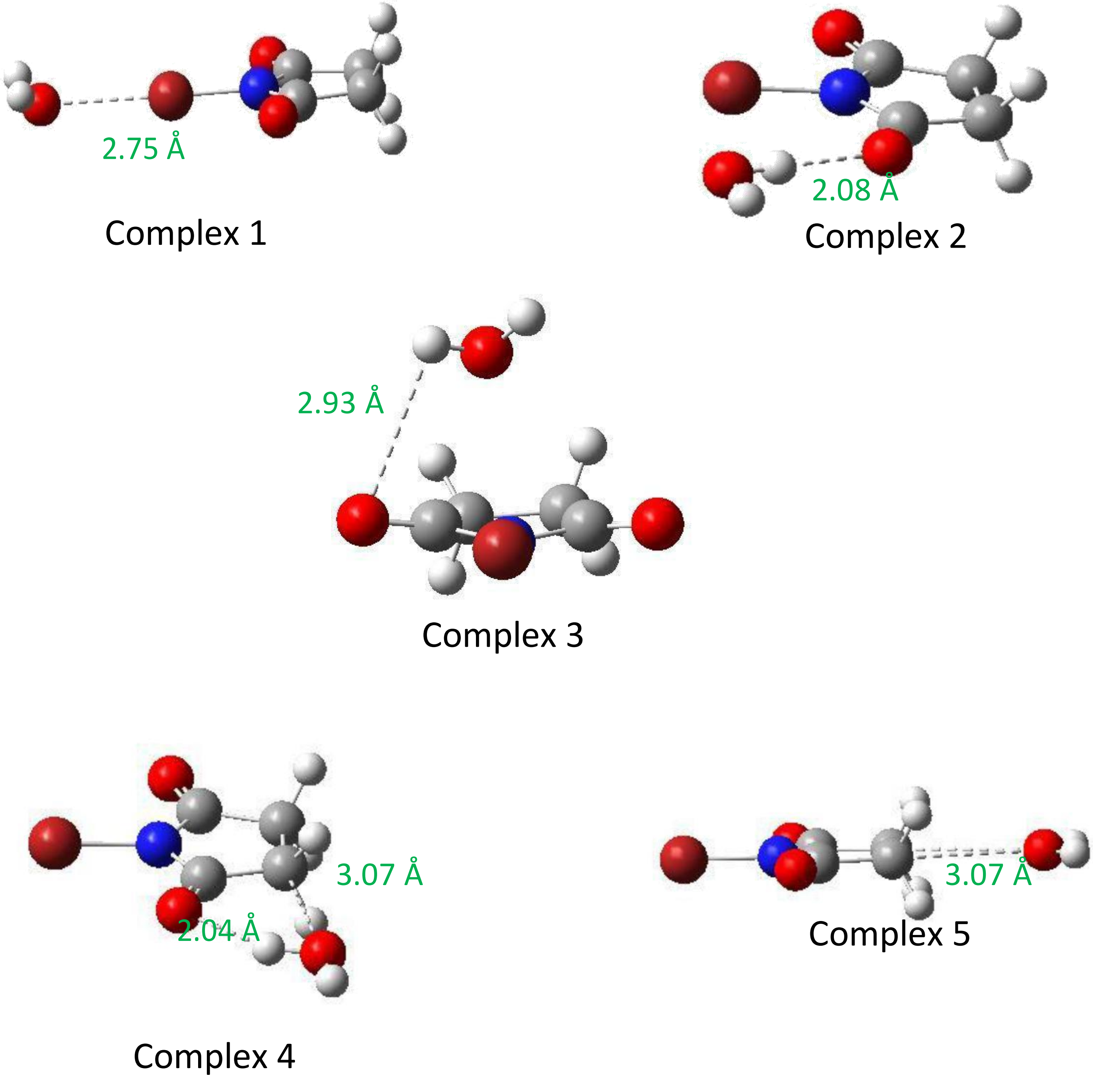

Complex 1

Complex 2

Complex 3

Complex 4

Complex 5

Figure 3.3: Optimized geometries of NBS-H_2O complexes at MP2/DGDVDZ level of theory. The intermolecular distances are also shown. .

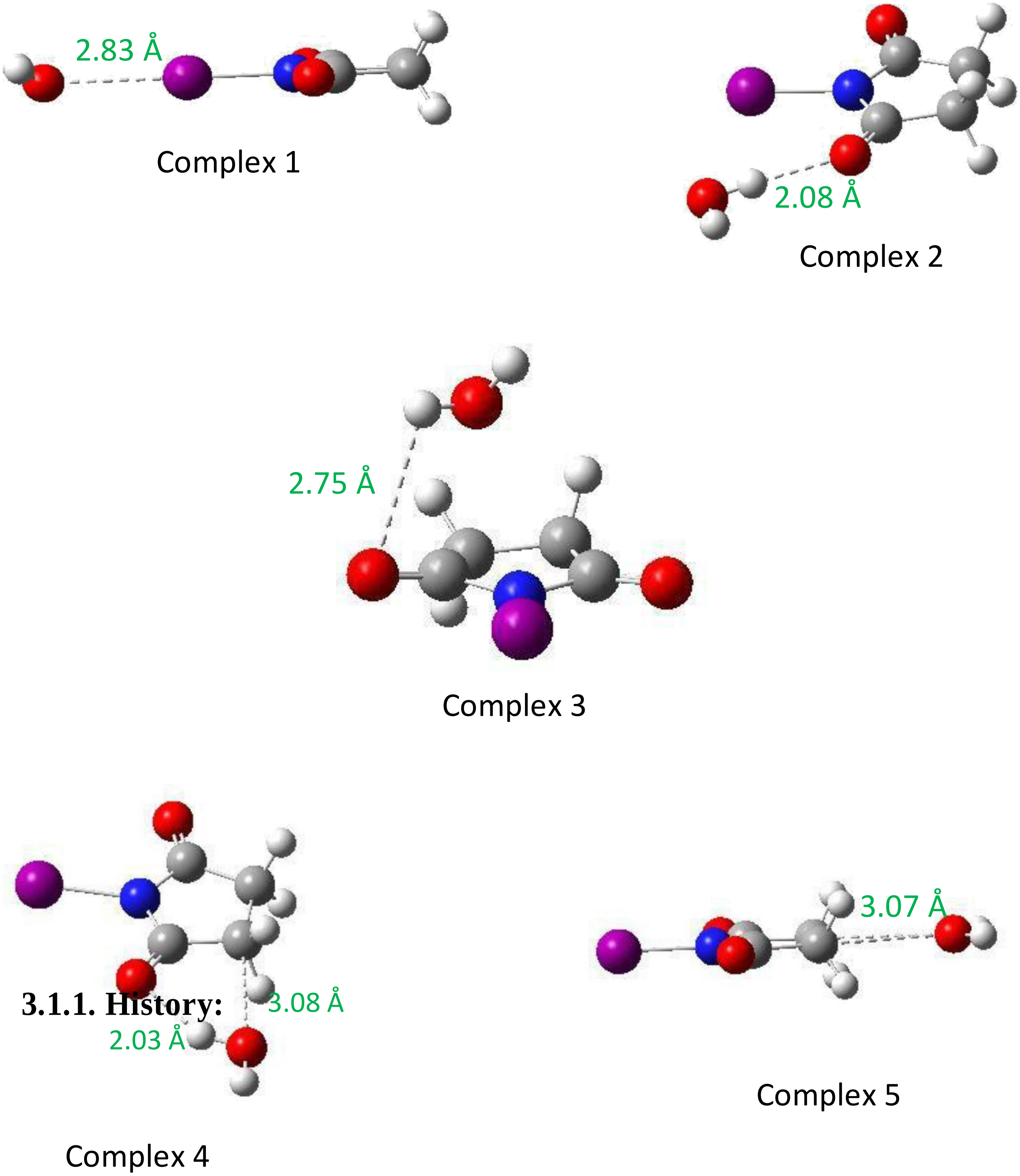

Complex 1

Complex 2

Complex 3

Complex 4

Complex 5

3.1.1. History:

Figure 3.4: Optimized geometries of NIS-H_2O complexes at MP2/DGDVDZ level of theory. Also shown are the intermolecular distances.

Table 3.1: Important geometrical parameters, bond length (Å) bond angles (°) and dihedral angels (°), for NBS-H_2O complexes were computed at the MP2/DGDZVP level. Labeling of atoms is shown in Figure 3.1.

Parameters for different optimized complex of NBS-H_2O									
Complex 1		Complex 2		Complex 3		Complex 4		Complex 5	
O_{13}-Br_{12}	2.7	O_{10}-H_{14}	2.0	O_{10}-H_{14}	2.9	O_{10}-H_{14}	2.0	O_{13}-H_6	2.9
H_{14}-O_{13}-Br_{12}	118.0	O_{13}-H_{14}-O_{10}	178.3	C_7-H_{14}	2.9	O_{13}-H_6	2.7	O_{13}-H_4	2.9
O_{13}-Br_{12}-N_9-C_7	-25.6	O_{13}-H_{14}-O_{10}-C_7	179.9	O_{13}-H_{14}-O_{10}	100.8	O_{13}-H_{14}-O_{10}	148.0	O_{13}-H_6-C_2	88.5
				O_{13}-H_{14}-N_9	65.9	H_6-O_{13}-H_{14}	79.8	H_{14}-O_{13}-H_6	148.1
				O_{13}-H_{14}-O_{10}-C_7	5.8	O_{13}-H_{14}-C_2	90.9	H_{14}-O_{13}-H_4	101.1
				O_{13}-H_{14}-N_9-Br_{12}	125.5	O_{13}-H_{14}-C_2-H_6	58.9	H_{14}-O_{13}-H_6-C_2	88.0
						O_{13}-H_{14}-O_{10}-C_7	-0.1	H_{14}-O_{13}-C_1-C_2	178.0

Table 3.2: Important geometrical parameters, bond length (Å) bond angles (°) and dihedral angles (°),for NIS,NIS-H_2O complexes, were computed at the MP2/DGDZVP level. Labeling of atoms is shown in Figure 3.2

Parameters for a different optimized complex of NIS-H_2O									
Complex 1		Complex 2		Complex 3		Complex 4		Complex 5	
O_{13}-I_{10}	2.8	O_{11}-H_{14}	2.1	O_{11}-H_{14}	2.7	O_{11}-H_{14}	2.0	O_{13}-H_6	2.9
H_{14}-O_{13}-I_{10}	119.6	O_{13}-H_{14}-O_{11}	175.1	C_7-H_{14}	2.8	O_{13}-H_6	2.7	O_{13}-H_4	2.9
O_{13}-I_{10}-N_9-C_7	-89.1	O_{13}-H_{14}-O_{11}-C_7	-179.6	O_{13}-H_{14}-O_{11}	106.0	O_{13}-H_{14}-O_{11}	149.1	O_{13}-H_6-C_2	88.4
				O_{13}-H_{14}-N_9	69.6	H_6-O_{13}-H_{14}	79.4	H_{14}-O_{13}-H_6	148.2
				O_{13}-H_{14}-O_{11}-C_7	5.2	O_{13}-H_{14}-C_2	91.8	H_{14}-O_{13}-H_4	101.3
				O_{13}-H_{14}-N_9-I_{10}	123.7	O_{13}-H_{14}-C_2-H_6	60.6	H_{14}-O_{13}-H_6-C_2	88.0
						O_{13}-H_{14}-O_{11}-C_7	1.0	H_{14}-O_{13}-C_1-C_2	-179.9

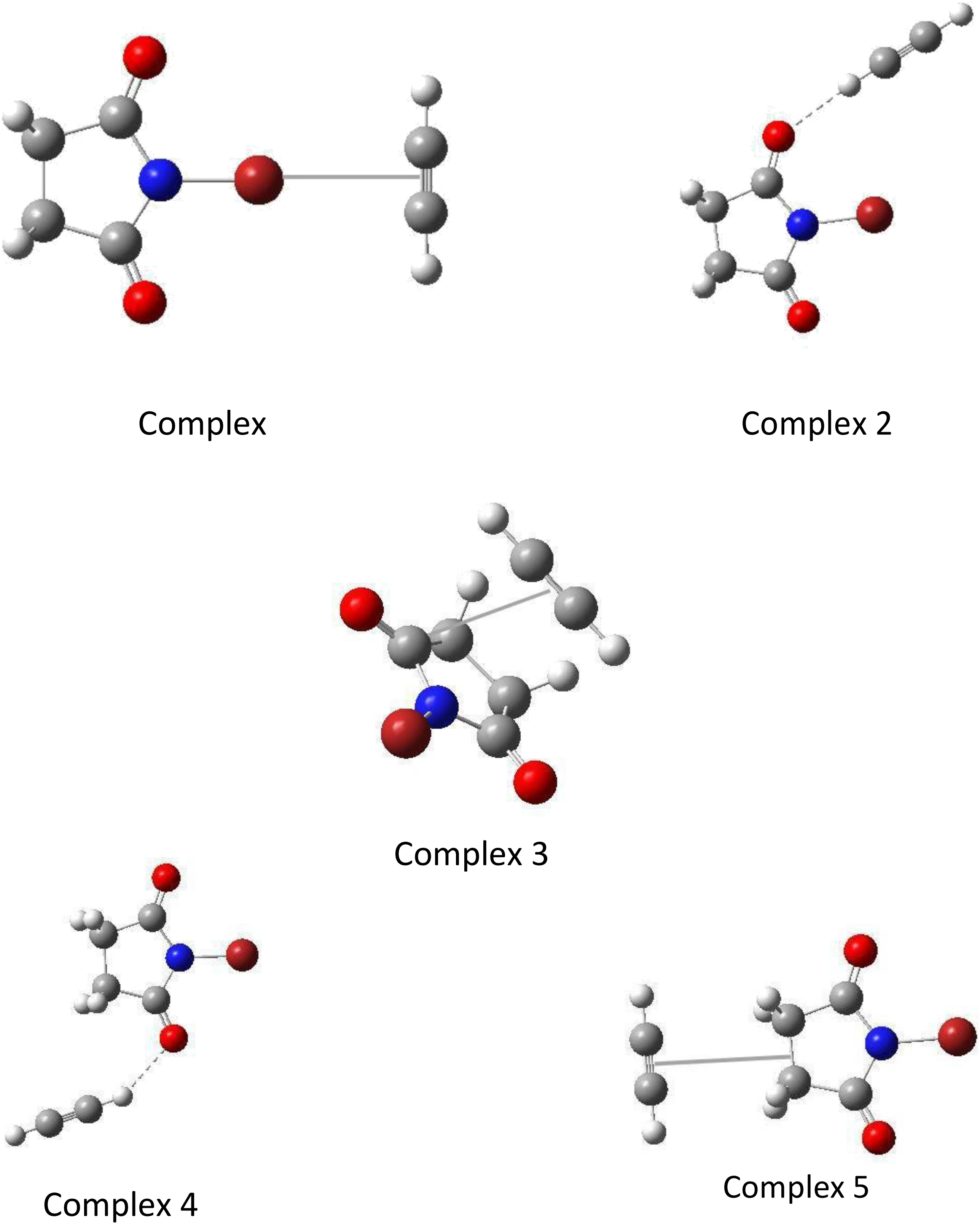

Complex

Complex 2

Complex 3

Complex 4

Complex 5

Figure 3.5: Optimized geometries of NIS-acetylene complexes at MP2/DGDVDZ level of theory

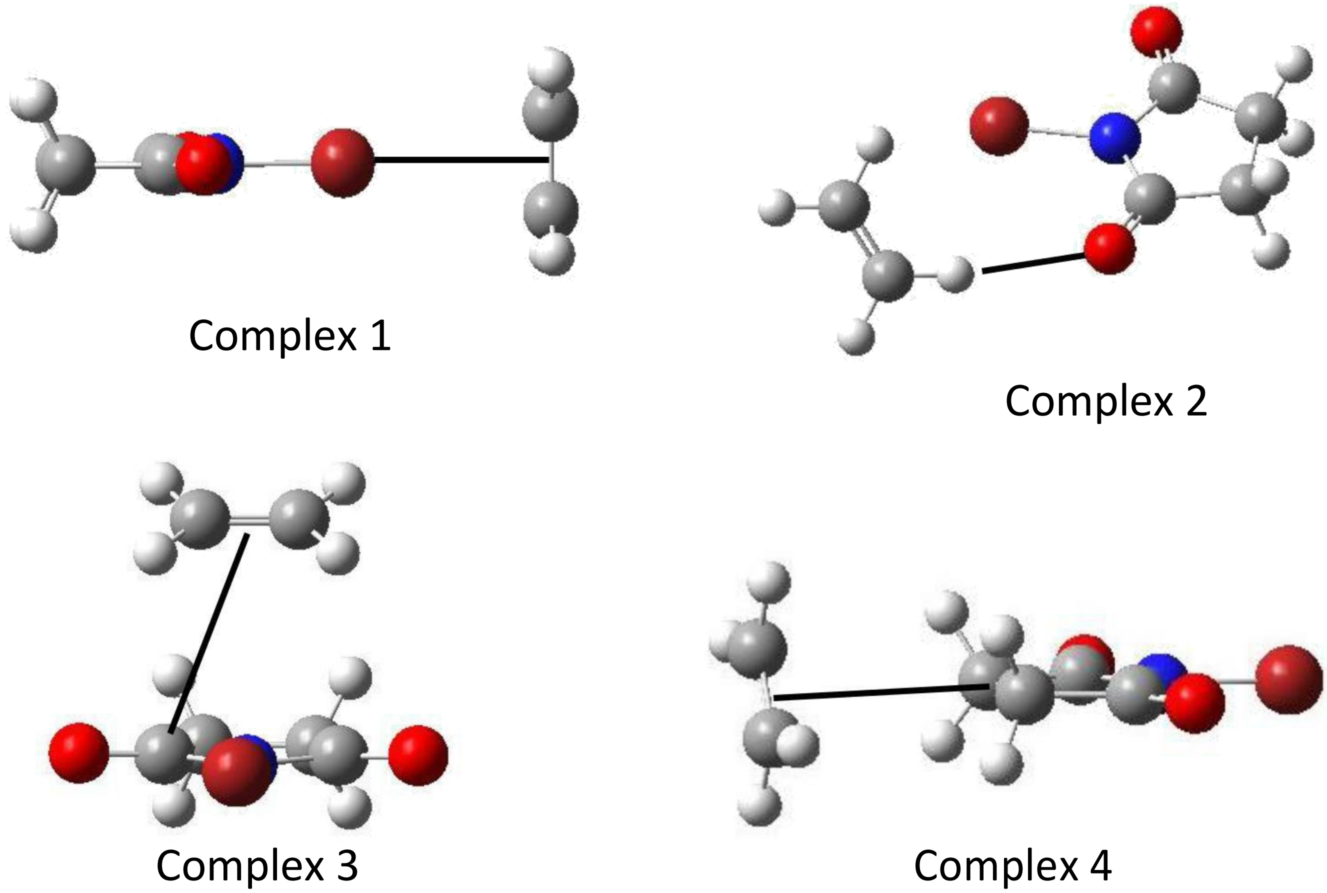
Complex 1

Complex 2

Complex 3

Complex 4

Figure 3.6: Optimized geometries of NIS-ethylene complexes at MP2/DGDVDZ level of theory

3.2 Experimental Details

NBS was used without any further purification. MilliQ Water (16-18 Ω – not correct) was used after subjecting it several freeze-pump-thaw cycles. Ar and N_2 (Sigma & Gasses, 99.999%) were used as the matrix gases. The desired matrix to water ratios were prepared using standard manometric[33] procedures.

At the outset, NBS was deposited on a KBr window together with matrix gas to record the infrared spectrum of NBS. Likewise, water was deposited in the matrix to record the spectrum of the uncomplexed precursor. To study the interaction between the NBS and water, both submolecules were codeposited on the window, and the spectra were then recorded. Since NBS is solid, it was deposited using a heated nozzle. The NBS vapor produced were swept away onto the cold substrate window by flowing matrix gas. As NBS was deposited in the matrix using a transpiration[34] method, the exact amount of sample to matrix ratio for NBS, could not be estimated. However, concentration dependence experiments indicated that we were depositing monomeric NBS.

The matrix isolation experiments of NBS were performed at varying concentration by varying the heating temperature. The dimer or polymer was not formed while depositing the NBS were taken care by keeping the concentration of NBS not too high. The sample to matrix ratio of water was varied from 0.7:1000 to 3.1:1000. The sample and matrix gas were deposited on to the cold KBr window at a deposition rate of ~3 mmol/hr using an effusive nozzle. After the deposition, the matrix temperature was raised to 25 K for the N_2 matrix while in the case of Argon 32 K, maintained at this temperature for 30 to 45 minutes and then recorded the spectra. The matrix was recooled to 12 K and spectra of annealed matrix was recorded. The matrix was annealed, to encourage the diffusion of the precursor and the formation of the complex, which can be identified by observing new product features in the spectra.

3.3 Results

3.3.1 Computational Results

Both the precursors i.e. NBS/NIS and water are a multifunctional molecule, with both of them presenting proton acceptor and proton donor sites. The NBS/NIS can act as proton acceptor through carboxyl π clouds and at the bromine/iodine. In addition the σ-hole can act as an electrophilic center. Also the H_2O can also act as an amphiprotic molecule, by serving both as a proton donor or an acceptor. Similarly, acetylene and ethylene can also act as a proton donor and proton acceptor through with π cloud.

The optimized geometry of five different complex as shown in above figures. This Complexes does not shows any negative frequency thus confirming that all the geometries are minima on the potential surface. The interaction energy was estimated got the various complexes. The interaction energies were also corrected for zero point energies (ZPE), and basis set superposition error (BSSE) at each level of theory. All interaction energies are shown in Table 3.3 and 3.4.

In the case of NBS-water complexes five different optimized complexes were found, at both level of theories. However in the case of NIS-water interaction at MP2/DGDZVP five and M06-2X/DGDZVP four different complex were found. Complex 4 was not optimized at the M06-2X level of theory in the case of NIS-water interactions.

Complex 1(n-σ^*_{N-Br}): The oxygen donates the lone pair to the sigma hole in front of the bromine atom.

Complex 2 (n-σ^*_{O-H}**):** The water molecule donates the proton to the Oxygen of Carboxyl group of NBS.

Complex 3 (n-σ^*_{C-O}): The water molecule donates the proton to the carboxyl (C=O) π cloud.

Complex 4(n- σ^*_{O-H} & n- σ^*_{C-C}): The water donates a proton to the carbonyl oxygen of NBS and accepts a proton at its oxygen atom from the C-C.

Complex 5(n-σ^*_{C-C}): The oxygen of water donates the lone pair to the antibonding orbital of C-C bond.

Also in the case of NBS-acetylene and NIS-acetylene the five different optimized complexes were found at the same MP2 level of theory. While NBS-ethylene and NIS-ethylene only showed four different optimized complexes. Complex 4 was the one who wasn't found. All the interactions present in the case of NBS-H_2O were the same instead of lone pair of oxygen, π cloud were present.

In the case of the NBS-H2O system, Complex 4 has the largest interaction energy at both level of theories, M06-2X and MP2, after BSSE correction. In the case of NIS-water system, complexes 1 and 4 are nearly isoenergetic and most stable complex at the MP2 level. At the M06-2X level complex 1, the halogen bonded complex was found to be the most strongly bond. Complex 4 was not optimized at this level. As the system changes to NBS-acetylene complex 3 becomes more stable and the gap between complex 1 and most stable complex was decreased in comparison to NBS-water. In the case of NBS-ethylene the most stable complex was found as complex 3 but the difference between the complex 1 and most stable was almost came to 0.2 kcal. (Which is not much significant difference as in terms of ab-initio calculation). Instead of NBS, NIS came into the picture with ethylene then the most stable complex was found was complex 1(halogen bonded).

In the case of NIS-ethylene, it is confirmed that the halogen bond interaction was the strongest among other interactions. While in the case of NBS-water the halogen bonded interaction is not indicated to be the most strongly bound system but the difference is too less. Therefore the halogen bond complex found to be strongly bound to influence the chemistry of this system. The halogen bonded system can well serve as the gateway complex for the bromination reaction.

Table 3.3: Interaction energies for the different NBS-H_2O and NIS-H_2O complexes at two different levels of theory. Interactions energies have been given as Raw/ZPE/BSSE energies (kcal/mol).

	NBS-water		NIS-water	
	MP2/DGDZVP (RAW/ZPE/BSSE)	M06/DGDZVP (RAW/ZPE/BSSE)	MP2/DGDZVP (RAW/ZPE/BSSE)	M06/DGDZVP (RAW/ZPE/BSSE)
Complex 1	**-5.6/ -4.4/ -4.3**	**-6.2/ -4.5/ -5.8**	**-7.2/ -5.9/ -5.5**	**-8.2/ -7.0/ -7.5**
Complex 2	-5.6/ -4.0/ -4.2	-6.2/ -4.7/ -5.6	-5.5/ -3.9/ -4.1	-6.3/ -4.9/ -5.7
Complex 3	-7.8/-6.3/-4.7	-9.1/-7.6/-7.8	-7.7/-6.1/-4.6	-9.0/-7.4/-7.5
Complex 4	-7.4/ -5.7/ -5.5	-8.5/ -6.8/ -7.8	-7.4/ -5.7/ -5.5	......
Complex 5	-4.2/ -3.3/ -2.7	-4.7/ -3.6/ -4.0	-4.1/ -3.2/ -2.5	-4.6/ -3.5/ -3.9

Table 3.4: Interaction energies for the different NBS-acetylene, NBS-ethylene, NIS-acetylene and NIS-ethylene complexes at MP2 levels of theory. Interactions energies have been given as Raw/ZPE corrected/BSSE energies (kcal/mol).

	NBS-acetylene	NBS-ethylene	NIS-acetylene	NIS-ethylene
	Energy (RAW/ZPE/BSSE)	Energy (RAW/ZPE/BSSE)	Energy (RAW/ZPE/BSSE)	Energy (RAW/ZPE/BSSE)
Complex 1	**-3.4/ -2.9/ -2.1**	**-4.0/ -3.4/ -2.4**	**-4.0/ -3.5/ -2.7**	**-5.0/ -4.2/ -3.1**
Complex 2	-3.9/ -3.1/ -2.6	-2.2/ -1.6/ -1.1	-3.9/ -3.1/ -2.7	-2.1/ -1.6/ -1.2
Complex 3	-5.3/-4.7/-2.9	-5.4/-4.7/-2.6	-5.4/-4.8/-3.0	-5.4/-4.8/-2.6
Complex 4	-4.1/-3.4/-2.8	**....**	-4.2/ -3.4/ -2.8	......
Complex 5	-2.3/ -1.9/ -1.2	-2.4/ -2.0/ -0.9	-2.6/ -1.9/ -1.1	-2.4/ -2.0/ -0.9

3.3.2 Experimental Results:

The spectra obtained for the NBS and NBS-water in N_2 matrix as shown in the Figure 3.5.Along with the experimental spectra computationally spectra of NBS, NBS-water complexes are also shown in the Figure 3.5. The spectral region depicted in the figure is between 1000 and 1900 cm^{-1}. The figure is divide into two region in which A) is the region of C=O stretching and B) is a region of skeleton mode which is combination of C-N and C-C starching motions. All experimental spectra are shown after annealing the matrix which is done at 25K. All the computed feature are appropriately scaled for a comparison of computational and experimental features. Scaling factor for a particular region in the spectrum is calculated by dividing the experimental wavenumber and for the monomer feature by the computed wavenumber for the same mode of the monomer.

The observed feature of C=O stretching occurs at 1746.1cm^{-1} in the N_2 matrix. On co-deposition of the water and NBS a red shifted feature at 1705.6cm^{-1} was observed which is due to different complexes that have been found computationally. This feature was broad because the high amount of water. Computationally also indicate the C=O stretch to be red shifted in both of the complex 4(most stable complex) and complex 1(halogen bond). The feature of CO stretch in complex 4 and complex 1 both were almost the same respectively 1737.6cm^{-1} and 1737.5 cm^{-1} as shown in the figure 3.5.

The other feature of NBS which was the combination of C-C and C-N stretch occurs at the 1167.0cm^{-1} in N_2 matrix. While in the case of that feature blue shifted and was found to be at 1195.2 cm^{-1}. Also the computationally feature in complex 1 and complex 4 were blue shifted. Complex 4 was blue shifted by 4.8 cm^{-1}, while complex 1 was blue shifted by 16cm^{-1}. This difference of the blue shift of the complexes is significant to distinguish them in experimental observed spectrum. But the experimental feature of NBS-H_2O was broad due to the high amount of the water. Therefore experimentally complex 1 and complex 4 aren’t distinguishable. However, the above features result clearly indicates the experimental evidence of interaction present between NBS and water molecule.

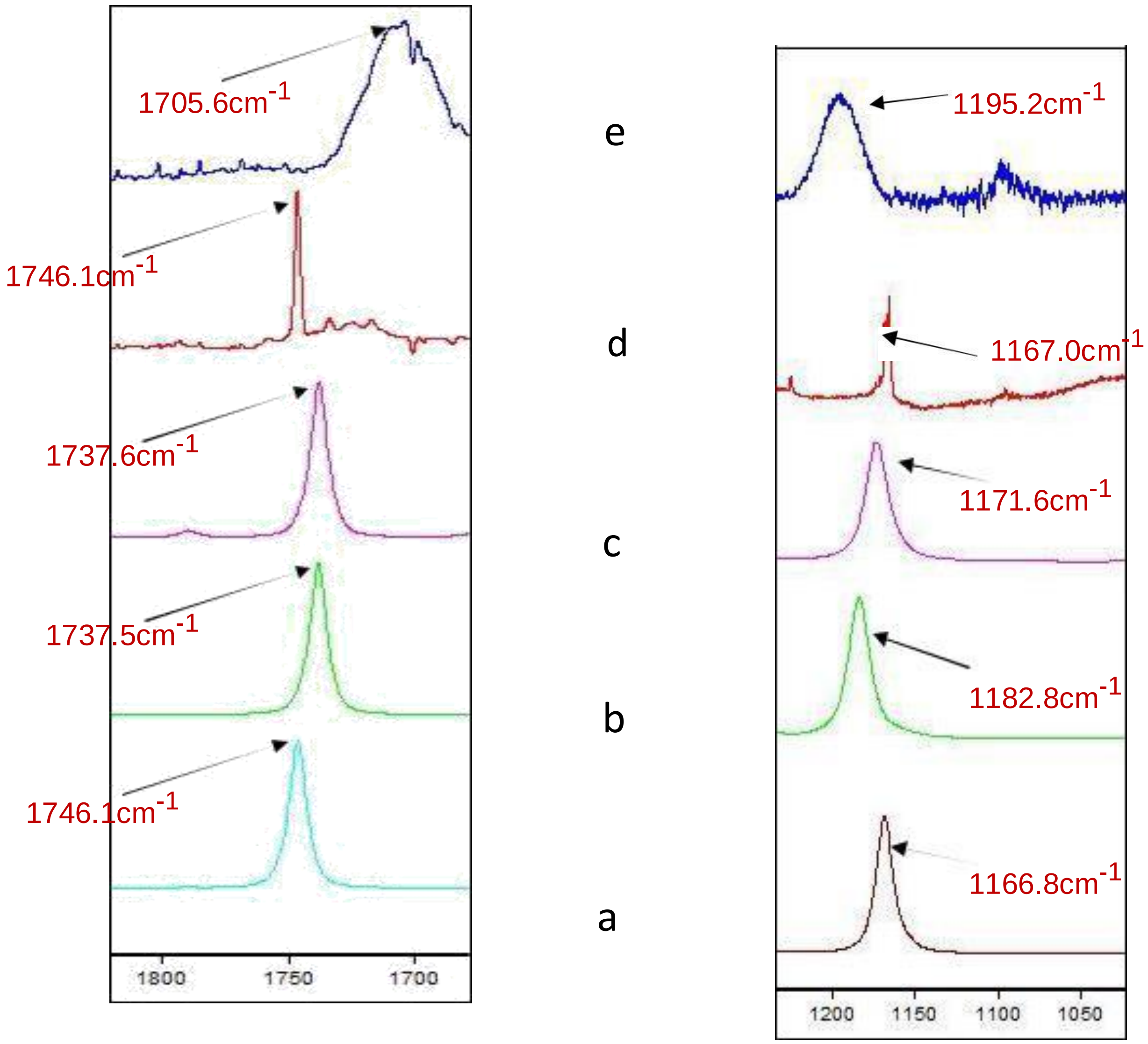

A) Region of C=O stretching

B) Region of skeleton mode

Figure 3.7: Spectra of NBS and NBS-water complex in N_2 matrix in two parts A) region of C=O stretching B) skeleton mode with C-C stretching mode being dominant (a) Computed spectra of NBS, (b) computed spectra of NBS-water complex 1 (c) Computed spectra of NBS-water complex 4 (d) experimental spectra of NBS in N_2 matrix (e) experimental spectra of NBS-water in N_2 matrix.

3.4 Discussion

3.4.1 AIM Analysis

The atom in molecule (AIM) theory based on the model which defines the chemical bonding or structure of molecule based on the topology of the electron density. The AIM2000 software was used to find out the interaction present between the NBS-water and NIS-water. The confirmation was done by finding out a bond critical point. The wave function generated by the G09 using optimized geometries was used as an input file for AIM2000. The bond critical point (3, -1) and ring critical point (3, +1) was found in the NBS-water and NIS-water interaction and shown in Figure 3.7 & 3.8 respectively.

In Figure 3.7 & 3.8, two types of critical points are present. The red dot represents the bond critical point while the yellow dot represents the ring critical point. Along with those various topological parameters were also calculated such as charge density ρ (r_c), eigenvalues of the Hessian matrix ($\lambda_1, \lambda_2, \lambda_3$), lagrangian kinetic energy (G) and the Laplacian ($\nabla^2\rho$) at bond critical points were shown Table 3.4 & 3.5. All these parameters were used in to calculate the interaction energy corresponding to the one bond critical point. Other than complex 1 all had two intermolecular bonds critical point. The calculated interaction energy by each bond critical point would determine the type of interaction was more contributing to stabilizing the complex. All the Laplacian ($\nabla^2\rho$) values were found positive; this indicated that interaction was closed shell type. The interaction energy was calculated using Espinosa's method[7] were listed in Table 3.4 & 3.5 as ΔE_{AB},

In NBS-water and NIS-water, the most stable interaction was present in complex 4. The most stable interaction was between C=O and O-H, and the strength of the interaction was 5.3 kcal were listed in Table 3.4 & 3.5. The second most stable interaction was present in complex 1, which denotes the halogen bonding, involves a lone pair of oxygen going into the sigma hole. The weakest interaction energy was shown by complex 5.Their strength of interaction was 1.7 kcal. The only major difference between NBS-water and NIS-water was the number of a bond critical point in complex 2 and complex 3. In case of NBS, there was two while in other only one bond critical point was found. Intermolecular Ring critical was also found in all the complexes except complex 1 in NBS, While in NIS it was found in only complex 4 and complex 5. In every case, there were two bonds critical point present ring critical point was also present there.

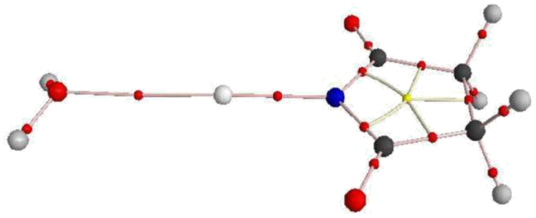

Complex 1

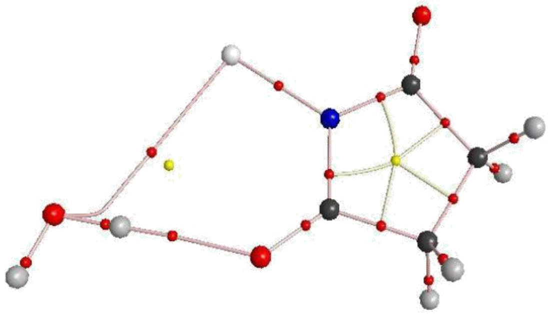

Complex 2

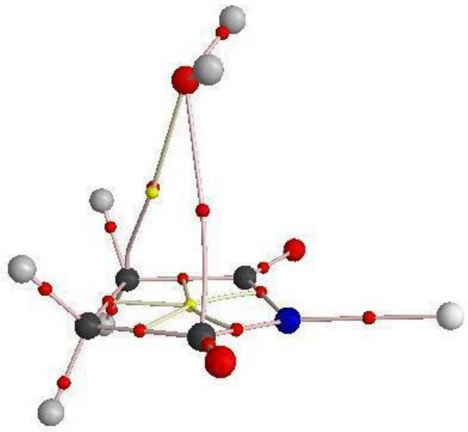

Complex 3

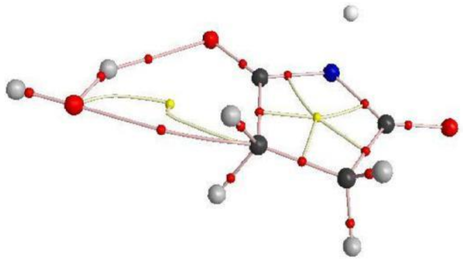

Complex 4

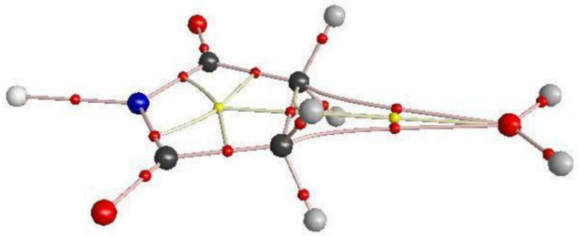

Complex 5

Figure 3.8: AIM analysis was carried on the optimized geometries of NBS-water at MP2/DGDZVP level of theory.

Complex 1

Complex 2

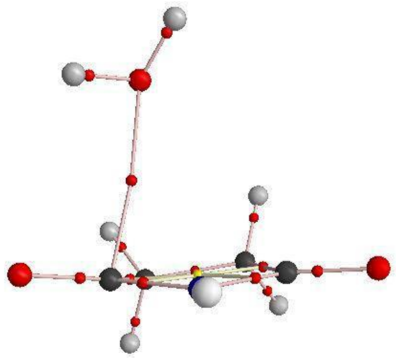

Complex 3

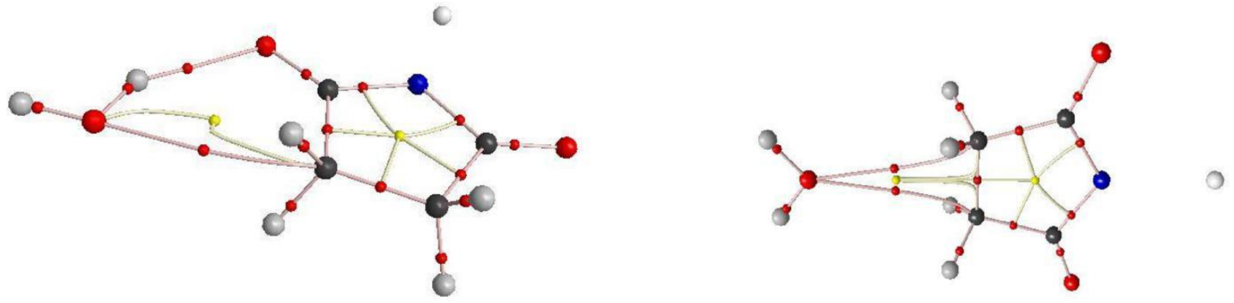

Complex 4

Complex 5

Figure 3.9: AIM analysis was carried on the optimized geometries of NIS-water at MP2/DGDZVP level of theory.

Table 3.5: Topological parameter by AIM analysis of the NBS-water complexes. All quantities are expressed in the atomic unit (a.u.) except interaction energies. They are in kcal unit.

		ρ (r_c)	$\nabla^2\rho$	λ_1	λ_2	λ_3	G	ΔE_{AB}	Total E_{int}
Complex 1		0.0196	0.0739	-0.0147	-0.0131	0.1018	0.0167	-4.72	-4.73
Complex 2	bcp1	0.0174	0.0689	-0.0224	-0.0222	0.1136	0.0154	-4.29	
	bcp2	0.0051	0.0225	-0.0033	-0.0011	0.0270	0.0044	-0.99	-5.9
Complex 3	bcp1	0.0118	0.0450	-0.0077	-0.0045	0.0573	0.0100	-2.75	
	bcp2	0.0078	0.0345	-0.0027	-0.0007	0.0381	0.0072	-1.82	-4.58
Complex 4	bcp1	0.0208	0.0804	-0.0274	-0.0271	0.1350	0.0183	-5.19	
	bcp2	0.0072	0.0330	-0.0048	-0.0007	0.0386	0.0066	-1.59	-6.78
Complex 5	bcp1	0.0075	0.0327	-0.0038	-0.0008	0.0374	0.0068	-1.73	
	bcp2	0.0075	0.0327	-0.0038	-0.0008	0.0374	0.0068	-1.73	-3.46

Table 3.6: Topological parameter by AIM analysis of the NBS-water complexes. All quantities are expressed in the atomic unit (a.u.) except interaction energies. They are in kcal unit.

		ρ (r_c)	$\nabla^2\rho$	λ_1	λ_2	λ_3	G	ΔE_{AB}	Total E_{int}
Complex 1		0.0211	0.0716	-0.0141	-0.0125	0.0983	0.0168	-4.98	-4.98
Complex 2		0.0172	0.0694	-0.0220	-0.0220	0.1135	0.0155	-4.29	-4.29
Complex 3		0.0122	0.0468	-0.0073	-0.0064	0.0606	0.0104	-2.89	-2.89
Complex 4	bcp1	0.0213	0.0819	-0.0283	-0.0279	0.1383	0.0187	-5.34	
	bcp2	0.0072	0.0326	-0.0050	-0.0017	0.0394	0.0065	-1.56	-6.86
Complex 5	bcp1	0.0075	0.0325	-0.0038	-0.0008	0.0372	0.0068	-1.72	
	bcp2	0.0075	0.0325	-0.0038	-0.0008	0.0372	0.0068	-1.72	-3.44

3.4.2 NBO analysis

The natural bond orbital analysis was performed on the optimized complex of NBS-water and NIS-water. The natural bond orbital calculated several factors, but here we just listed some of them in Table 3.6 and 3.7 which are important in terms of defining the interaction between two monomers. Second order perturbation (E), orbital energy difference between acceptor and donor [E(j)-E(i)] and the overlap between the donor and acceptor orbital [F(i,j)] (it is the off-diagonal terms of Fock matrix element). The strongest interaction was observed in the complex 1, oxygen (H_2O) donates the electron density from lone pair to the sigma hole (antibonding orbital of N-Br) created by NBS. The most stable complex was found to be using G09 interaction energy with BSSE correction listed in Table 3.3 wasn't the most stable after adding all primary interaction. Here the second order perturbation energy was calculated using below formula[7]

$$\Delta E_{ij} = \frac{q(i).F(i,j)^2}{E(j)-E(i)}$$

Where q (i) is the donor orbital occupancy, F(i,j) Fock matrix off-diagonal element, E(i) and E(j) are the diagonal elements of Fock matrix, and the ΔE_{ij} is the second order perturbation energy. In both NBS and NIS, There was two types of interaction was present in the complex 2 and complex 3 by NBO analysis which wasn't seen by AIM analysis in NIS-water interaction. The interaction was very weak in comparison to other interactions present in the complex might be the reason aim analysis couldn't give that information.

In the case of NBS complex, 4 was almost equal to the Complex 1, while in NIS-water scenario complex 1 was way ahead in terms of stability than to complex 4. As we already knew from the literature[8] the sigma hole size is bigger in Iodine than Bromine. If the size of the sigma hole is big, then the chances of donating the electron density would be greater. This also confirms that the interaction is happening between the lone pair of Oxygen and the sigma hole. The interaction is not the strongest, but it is considerable. Now in the next section which type of interaction is more contributing to the stability of the complex will be Figure out by the energy decomposition analysis in the next section.

Table 3.7: NBO analysis of NBS-water was carried at the MP2/DGDZVP level of theory. The atom number was the same as indicated in Fig. 3.1. E_2 is the second order perturbation (kcal/mol), E(j)-E(i) energy difference between donor(a.u.) and acceptor orbital and F(i,j) overlap matrix element(a.u.)

	Donor NBO	Acceptor NBO	E_2	E(j) – E(i)	F(i,j)
Complex 1	n(2) O_{13}	σ*(1) N_9 - Br_{12}	**7.52**	**1.00**	**0.078**
Complex 2	n(1) O^{11}	σ*(1) O_{13} - H_{14}	3.00	1.79	0.066
	n(2) O_{11}	σ*(1) O_{13} - H_{14}	2.65	1.29	0.054
	n(1) N^9	σ*(1) O_{13} - H_{14}	0.65	1.22	0.025
Complex 3	n(2) O^{13}	σ*(1) C^7- O_{10}	3.00	1.01	0.051
	σ(1) O_{13}-H_{14}	σ*(1) C_7 - O_{10}	0.95	1.19	0.031
	σ(1) O^{13}-H^{14}	σ*(1) C_7- O_{10}	0.94	1.54	0.028
Complex 4	n(1) O^{10}	σ*(1) O_{12} - H_{13}	2.32	1.75	0.057
	n(2) O_{10}	σ*(1) O_{12} - H_{13}	4.24	1.25	0.067
	n(2) O^{13}	σ*(1) C^1 - C^2	0.77	1.47	0.30
Complex 5	n(2) O^{13}	σ*(1) C^1 - C^8	1.25	1.53	0.039
	n(2) O^{13}	σ*(1) C^1 - C^7	1.25	1.53	0.039

Table 3.8: NBO analysis NIS-water was carried at the MP2/DGDZVP level of theory. The atom number was the same as indicated in Fig. 3.1. E_2 is the second order perturbation (kcal/mol), E(j)-E(i) energy difference between donor(a.u.) and acceptor orbital and F(i,j) overlap matrix element(a.u.)

	Donor NBO	Acceptor NBO	E(2)	E(j) – E(i)	F(i,j)
Complex 1	n(2) O^{13}	σ*(1) N_9 - I_{10}	**10.22**	**0.97**	**0.09**
Complex 2	n(1) O^{11}	σ*(1) O_{13} - H_{14}	4.04	1.78	0.076
	n(2) O^{11}	σ*(1) O_{13} - H_{14}	3.29	1.30	0.060
	n(1) N^9	σ*(1) O_{13} - H_{14}	0.62	1.22	0.025
Complex 3	n(2) O^{11}	σ*(1) C^7- O_{11}	3.40	1.01	0.054
	σ(1) O_{13} -H_{14}	σ*(1) C^7- O_{11}	1.11	1.19	0.034
Complex 4	n(1) O^{11}	σ*(1) O_{13} - H_{14}	2.46	1.75	0.059
	n(2) O^{11}	σ*(1) O_{13} - H_{14}	4.39	1.25	0.068
	n(2) O^{13}	σ*(1) C^1 - C^2	0.74	1.47	0.029
Complex 5	n(2) O^{13}	σ*(1) C^1 - C^8	1.24	1.53	0.039
	n(2) O^{13}	σ*(1) C^1 - C^7	1.24	1.53	0.039

3.4.3 EDA analysis

The energy decomposition analysis (EDA) was performed on all the NBS-water and NIS-water optimized complexes to determine the contribution of electrostatic, exchange, repulsion, dispersion and polarization energy towards the total interaction energy. All the results have been listed in table 3.8 and 3.9 respectively for NBS-water and NIS-water. The Localized molecular orbital energy decomposition analysis (LMO-EDA) was performed using GAMESS software using optimized geometries from Gaussian09.

It is quite clear from Table 3.8 that electrostatic energy (E_{elect}) and exchange energy (E_{exch}) part is more dominating than others. The most stable complex 4 has the highest value of the electrostatic and exchange energy, but when it comes to polarization, the highest value of polarization (E_{pol}) energy was found to be in complex 1. The same case had been seen in the dispersion (E_{dis}) energy too. This was a clear indication that electrostatic contribution in hydrogen bonding versus halogen bonding varies according to the type of interaction in NBS-water and NIS-water.

The polarization and dispersion energy plays a significant role in halogen bonding along with the electrostatic energy. As we know by literature[9] MP2 level of theory incorporates dispersion correction in comparison to M06-2X. There is another confirmation that for halogen bonding MP2 level of theory is the best choice due to its dispersion correction. The total interaction energy (E_{total}) follows the trend of E_2 from the NBO analysis. Complex 1 and 4 were almost equal in energy in NBS-water, while in NIS-water complex 1 is most stable. We see the pattern in energy while going from NBS to NIS in complex 1. We saw every energy was rising except Dispersion energy. It remains constant.

Table 3.9: LMO-EDA analysis of the NBS-water complexes at MP2/DGDZVP level of theory. All the energies are in kcal/mol.

	E_{elect}	E_{exch}	E_{rep}	E_{ool}	E_{dis}	E_{total}
Complex 1	**-9.14**	**-10.98**	**19.47**	**-2.58**	**-1.11**	**-4.34**
Complex 2	-7.11	-6.79	11.73	-1.65	-0.35	-4.17
Complex 3	-10.17	-10.01	16.93	-1.49	-0.65	-5.39
Complex 4	-10.51	-10.01	17.47	-2.20	-0.40	-5.66
Complex 5	-4.21	-4.22	6.89	-0.60	-0.32	-2.51

Table 3.10: LMO-EDA analysis of the NBS-water complexes at MP2/DGDZVP level of theory. All the energies are in kcal/mol.

	E_{elect}	E_{exch}	E_{rep}	E_{ool}	E_{dis}	E_{total}
Complex 1	**-12.87**	**-15.76**	**28.26**	**-3.95**	**-0.91**	**-5.22**
Complex 2	-8.27	-10.26	17.79	-2.18	-0.58	-3.50
Complex 3	-9.71	-9.85	16.66	-1.48	-0.76	-5.16
Complex 4	-10.59	-10.18	17.77	-2.27	-0.41	-5.68
Complex 5	-4.23	-4.22	6.91	-0.62	-0.37	-2.53

Chapter 4

Conclusions

The complexes of NBS-water studied using matrix isolation Infrared spectroscopy and computation (ab-initio) calculation. NBS-ethylene, NBS-acetylene, NIS-water, NIS-acetylene and NIS-ethylene only studied using computation calculations. They were studied to determine the role of halogen bonding in the formation of Bromonium ion as intermediate in the mechanism of halogenation reaction using NBS. The ion formation occur using ethylene and NBS as precursors but we first look at the interaction using water due to its spectral feature. There were five different complexes were found in the investigation of both NBS-water and NIS-water interaction. Some complexes involves only one type of interaction while others have two type of interaction. There were all type of interaction present classical hydrogen bonding (n- σ*), H-π interaction and halogen bonding.

In NBS-water interaction complex 4 was most stable structure While in NIS-water interaction Complex 4 and Complex 1 was isoenergetic and found to be the most stable complex. When system changes from NBS to NIS only halogen bonded complex got affected while all other remains same in terms of stability. The complex 1 become -4.3kcal/mol to -5.5kcal/mol because NIS has bigger sigma hole than NBS given in the Figure 3.1.

In the case of NBS-ethylene most stable complex found was complex 3. The difference between the complex 1(halogen bonded) and the most stable complex was found to be 0.2 kcal/mol as shown in the figure 4.1. This energy difference between the two complexes was very less. This indicates that the halogen bonding is affecting the chemical reactivity of the halogenation reaction. The sigma hole is playing a big role in the formation of Bromonium ion in the mechanism of halogenation reaction.

The stability of the NBS-ethylene complexes has been shown in the Figure 4.1. NBO and AIM confirms that the type of interaction was halogen bonded and clearly involving the σ hole in the complex 1 in all the cases. EDA analysis confirms the electrostatic behavior of the interaction and in some amount polarization and dispersion also plays a part in halogen bonding too.

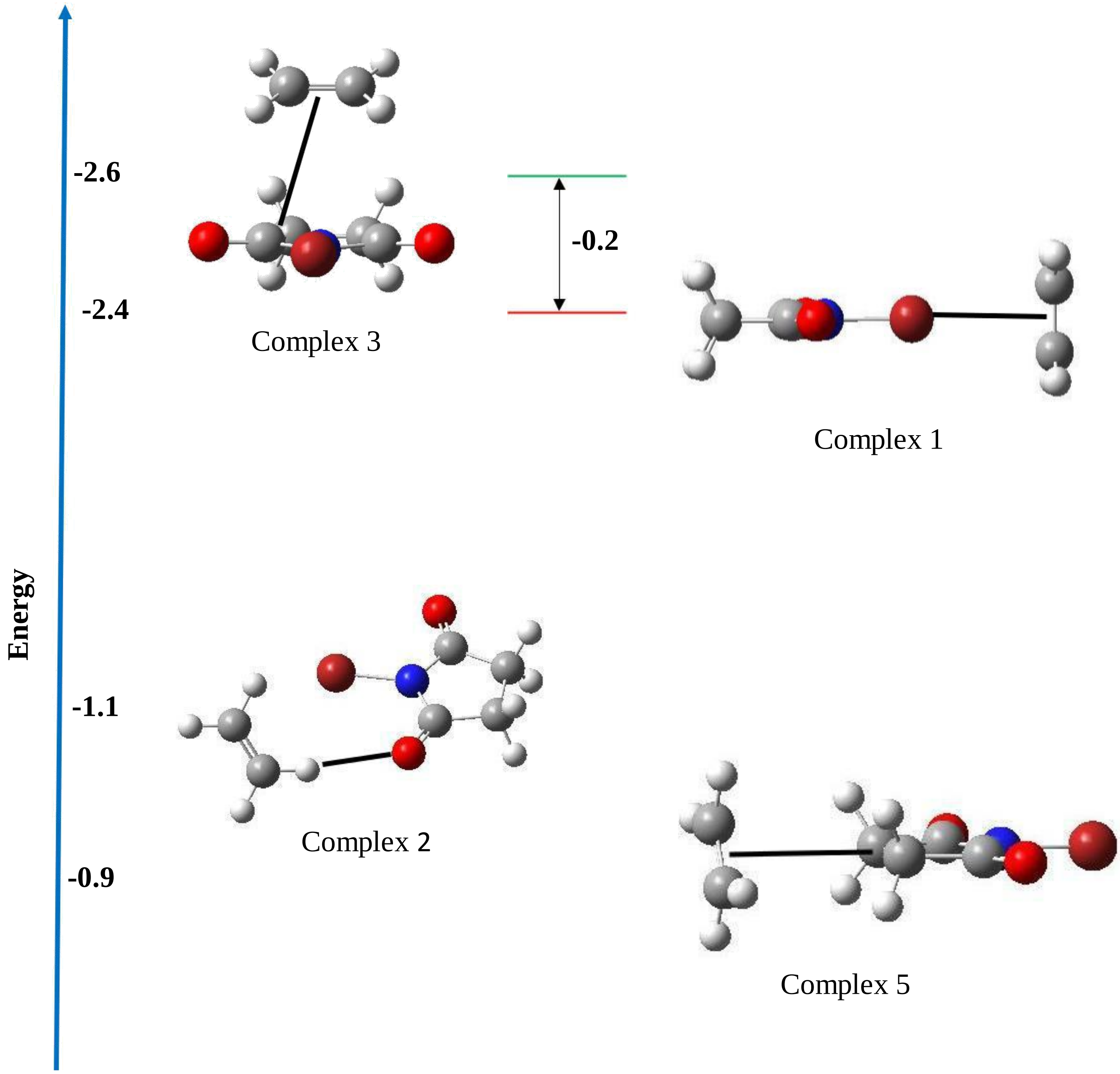

Figure 4.1: Complexes of NBS-ethylene in energy ordering. All the energies are BSSE corrected and are in kcal/mol.

The experimental results was found to be at good correlation with the computational results. The two spectral region of experimental results confirms that the NBS-water has good interaction but due to broadness of NBS-water distinguishability between complex 1(halogen bonded) and complex 4(most stable) wasn't found. Overall the experimental and computational results confirms that the halogen bonding playing significant role in the formation of Bromonium ion. The halogen bonded complex can serve as gateway complex for the halogenation reaction.

References

[1] Intermolecular bonding (2019, March 08). Chemical bond. Retrieved from https://en.wikipedia.org/wiki/Chemical_bond.

[2] Desijaru GR, Ho PS, Kloo L, Legon AC, Marquardt R, Metrangolo P, Politzer P, Resnati G, Rissanen K, (**2013**). *Pure Appl. Chem*. 85 (8): 1711–1713.

[3] Politzer P, Lane P, Concha MC, Ma YG, Murray JS(**2007**) *J Mol Model* 13:305-311.

[4] Koohi A. M., Mahdavifar Z., Noorizadeh S., *ChemistrySelect* **2017**, 2, 2713.

[5] Mulliken R.S, (**1950**), *J. Am. Chem. Soc.,* 72 (1): 600.

[6] Hassel O, Hvoslef J, Vihovde E, Hadler, Sörensen, Nils Andreas (**1954**), *Acta Chem. Scand*., 8: 873.

[7] Dumas, J.-M.; Peurichard, H.; Gomel, M. (**1978**) *J. Chem. Res*. (S). 2: 54–57.

[8] Politzer P, Murray JS, Clark T, (**2010**) *Phys. Chem. Chem. Phys*. 101: 16789–16794.

[9] Clark, T.; Hennemann, M.; Murray, J. S.; Politzer, P. (**2007**) *J. Mol. Model*. 13 (2): 291–296.

[10] Auffinger P, Hays FA, Westhof E, Shing Ho P (**2004)** *Proc Nat Acad Sci* 101:16789-16794.

[11] Murray JS, Riley KE, Politzer P, Clark T (**2010**) *Aust J Chem* 63:1598-1607.

[12] Politzer P, Harris RR (**1970**) *J Am Chem Soc* 92:6451-6454.

[13] Victor L. Heasley, Charles L. Frye, Robert T. Gore Jr., and Paul S. Wilday *J. Org. Chem.* **1968**, 33, 6, 2342-2345.

[14] M.S. Kharasch, Frank R. Mayo *J. Am. Chem. Soc.*, **1933**, 55, pp. 2468–96.

[15] Halogenation using NBS (2011, June 10). Master Organic Chemistry RSS. Retrieved from https://www.masterorganicchemistry.com/2011/06/10/reagent-friday-nbs-n-bromo-succinimide/.

[16] Beger J, (1991) J. Prakt. Chem. 333 (5): 677–698.

[17] Gaussian Inc. – Gaussian09, Revision A.02.

[18] Bader R. F. W., Atoms in Molecules. A Quantum Theory, Clarendon Press, Oxford, **1994.**

[19] Schmidt, M. W.; Baldridge, K. K.; Boatz, J. A.; Elbert, S. T.; Gordon, M. S.; Jensen, J. H.; Koseki, S.; Matsunaga, N.; Nguyen, K. A.; Su, S.; Windus, T. L.; Dupuis, M.; Montgomery, J. A. *J. Comput. Chem.* **1993**, 14 (11) 1347– 1363.

[20] Whittle, E.; Dows, D.A.; Pimentel, G.C. *J. Chem. Phys.* Matrix Isolation Method for the Experimental Study of Unstable Species. **1954**, *22,* 1943.

[21] Norman, I.; Porter, G. Trapped Atoms and Radicals in a Glass 'Cage.' *Nature*, **1954**, *174*, 508-509.

[22] Sander, W.; Costa, P. Hydrogen Bonding Switches the Spin State of Diphenylcarbene from Triplet to Singlet. *Angew. Chem. Int. Ed.* **2014,** *53,* 1-5.

[23] Hobe, M. von; Stroh, F.; Beckers, H.; Benter, T.; Willner, H. The UV/Vis Absorption Spectrum of Matrix-Isolated Dichlorine Peroxide, ClOOCl. *Phys. Chem. Chem. Phys.* **2009**, *11*, 1571-1580.

[24] Cradock, S.; Hinchcliffe, A. J. Matrix Isolation: A technique for the study of reactive inorganic species; *Cambridge University Press*, Cambridge, **1975**.

[25] Hallam, H. E. *Vibrational Spectroscopy pf Trapped Species*, John Wiley and Sons, London,**1973.**

[26] Buckingham, S. D. *Proc. Roy. Soc. (London) A*, **1958**,248,169.

[27] Pavel Hobza, Zdenvik Halves, *Theor Chem Acc*., **1998**, 93:372-77.

[28] Eric D. Glendening; *J. Phys. Chem. A.* **2005**, 109, 11936-11940.

[29] N. Godbout, D. R. Salahub, J. Andzelm, and E. Wimmer, "Optimization of Gaussian-type basis sets for local spin density functional calculations. Part I. Boron through neon, optimization technique and validation," *Can. J. Chem.*, **70** (1992) 560-71.

[30] N. R. Kestner, *J. Chem. Phys*., 48, 252, **1968**.

[31] Boys, S. F.; Bernardi, F. The Calculation of Small Molecular Interactions by the Differences of Separate Total Energies.Some Procedures with Reduced Errors. *Mol. Phys.* **1970**, *19*, 553-566.

[32] A.R. Allouche, Gabedit - A graphical user interface for computational chemistry softwares, J. Comput. Chem., 32 (2011) 174-182.

[33] Franz Goldstein, John H. Gibbon, Jr., Frank F. Allbritten, Jr., and Joseph W. Stayman, Jr., The combined manometric determination of oxygen and carbon dioxide in the blood, in the presence of low concentrations of ethyl ether. *J. Biol. Chem.* **1950**, 182: 815.

[34] Hales, S., Vegetable Statics *Pr. Reg. Soc., Innys,* Woodward, London, **1727.**

[35] R.M. Bentwood, A.J. Barnes, W.J.Orville-Thomas, Studies of intermolecular interactions by matrix isolation vibrational spectroscopy: Self-association of water *J. Mol. Stru*. 1980, 391-404.

[36] E. Espinosa, E. Molins, C. Lecomte, *J. Chem. Phys.* **1998**, 170-173.

[37] C. Møller and M. S. Plesset, *Phys. Rev*. 46, 618 (**1934**).